Ocean Circulation Model Hindcasts of the 1982–83 El Niño: Thermal Variability along the Ship-of-Opportunity Tracks

D. E. HARRISON*,@,+ WILLIAM S. KESSLER@ AND BENJAMIN S. GIESE@

*NOAA/PMEL, Seattle, Washington
@School of Oceanography, University of Washington, Seattle, Washington
+Department of Atmospheric Science, University of Washington, Seattle, Washington

(Manuscript received 17 August 1987, in final form 21 June 1988)

ABSTRACT

Five different analyses of 1982–83 monthly average surface wind stress fields have been used to force an ocean general circulation model of the tropical Pacific, in a series of El Niño hindcast experiments, like the one reported by Philander and Seigel. Although there were prominent common departures from climatology in the surface wind stress field during 1982–83 according to each wind analysis, there are also very substantial differences between analyses. This study was done to investigate the sensitivity of such hindcasts to our uncertain knowledge of the surface wind stress field. We concentrate here on the behavior along the Pacific ship-of-opportunity tracks.

According to the ship-of-opportunity XBT data, the ocean underwent major changes during this period. The vertical temperature gradients and mixed layer temperatures, as well as the depth of the thermocline, underwent substantial changes. There were also major changes in the geostrophic flow of the major current systems, as revealed by upper ocean dynamic height differences. Comparing the hindcasts with observations, we find that the gross large-scale changes of the ENSO event—surface warming in the second half of 1982, continued warmth into 1983 and cooling in mid-1983, together with major thermocline depth changes—are found in each hindcast. However, major quantitative differences exist between each hindcast and the observations in at least some region for some time and some variable.

Within the waveguide, dynamic height changes generally are hindcast with quantitative skill using each wind stress field and the best hindcasts differ from the observations by only a few dyn-cm more than the estimated uncertainty in the observations. Such hindcast skill is unlikely to be fortuitous: evidently the major elements of the waveguide variability are forced by the 1982–83 surface wind stress field rather than evolving out of some aspect of the state of the ocean during late 1981. Sea surface temperature changes are generally hindcast with qualitative skill, but rms errors of 2–3°C are frequent. Subsurface temperature variability skill varies with hindcast, location and depth; skill is greatest in the thermocline.

Outside the waveguide, hindcast skill tends to be reduced, and varies greatly with location and hindcast. Quantitative hindcast skill is found near 10°S and 10°N in some hindcasts in the WP, and near 10°S in most hindcasts in the CP, but there is never quantitative skill in the NECC region. The most striking inconsistency found involves the behavior of the NMC hindcast in the region of the North Equatorial Counter Current. Wind stress curl-forced Ekman pumping appears to be a significant factor in the variations in the more successful hindcasts.

In almost every comparison, the range of hindcast results brackets the observations, suggesting that the model physics is plausible. Overall, the special research effort wind fields produced better dynamic height results than did the operational wind product fields, but the operational fields produced generally better waveguide SST results. Improved knowledge of the surface wind stress field (and its curl) is a minimum requirement if we are to assess more critically model performance, and to identify needed model improvements.

1. Introduction

The tropical Pacific warm event of 1982–83 was one of the strongest in the historical record, and followed a pattern of evolution quite different from that of the Rasmusson and Carpenter (1982) post-1950 composite El Niño–Southern Oscillation (ENSO) event. Although extremely anomalous conditions occurred in both the atmosphere and ocean and although observations were better than in any previous event, our understanding of the mechanisms responsible for the event remains very incomplete. The density of observations in space and time simply is not sufficient to permit direct diagnosis of these mechanisms, particularly for the processes important for air–sea interaction.

Although the ENSO phenomenon is fundamentally an aspect of the coupled ocean–atmosphere system, much remains to be learned about the behavior of the individual fluids treated as initial–boundary value problems with forcing imposed at the air–sea interface. Unfortunately, as the air–sea forcing is known only subject to considerable uncertainty, an important as-

Corresponding author address: Dr. D. E. Harrison, NOAA/PMEL, Bldg. 3, Bin C15700, 7600 Sand Point Way, NE, Seattle, WA 98115

pect of any such "hindcasting" effort is to try to assess the impact of these uncertainties on the hindcasts.

For ocean hindcasts one must have an approximation to the state of the ocean at the beginning of the hindcast period and must be able to impose or parameterize the surface fluxes of momentum, heat, and water over the period of interest. Recent efforts to estimate the uncertainty in monthly mean estimates of surface wind (e.g., Halpern 1982; Harrison et al. 1982; Luther and Harrison 1983; Harrison et al. 1984) indicate that any two available analyses of the tropical Pacific will likely have rms differences of roughly 2 m s^{-1} (in wind fields where the maximum monthly mean speed is likely to be 7–9 m s^{-1} and the minimum monthly mean wind may be near zero). Efforts to assess the likely uncertainty in monthly mean net surface heat flux suggest that the uncertainty generally will exceed 50 W m^{-2} (e.g., Niiler 1981) (in fields where typical climatological values range between zero and something over 100 W m^{-2}). Precipitation minus evaporation (the net water flux) is generally neglected, because it is poorly known.

Philander and Seigel (1985) made an ocean hindcast of the 1982–83 ENSO, in which surface wind stress was estimated from National Meteorological Center (NMC) 1000 mb wind field analyses, surface heat flux was parameterized in terms of sea surface temperature, an imposed air–sea temperature difference and surface wind speed, and liquid water flux was neglected. This hindcast was able to reproduce some significant aspects of the 1982–83 event in the equatorial ocean, and motivates the sensitivity studies described here.

Because the different monthly mean wind and pseudostress analyses differ so substantially from each other it is important to try to understand how these differences affect both our ability to hindcast situations like the 1982–83 event and to infer the dominant physical processes responsible for the changes that occurred during such events. Should certain aspects of the tropical Pacific upper ocean be determined largely by linear forced physics, it would be straightforward to explain model hindcast differences in these quantities simply in terms of the differences in the stress fields. However, there is good reason to expect that many quantities, sea surface temperature (SST) and near surface currents in particular, will be determined by nonlinear mechanisms (e.g., Schopf and Cane 1983; Schopf and Harrison 1983), and hence a priori estimates of differences in these quantities are not likely to be simple to make.

We here report results from an effort to investigate the sensitivity of Philander and Seigel (1985) style hindcasts of the 1982–83 ocean ENSO event to our uncertain knowledge of the monthly average wind stress field over the tropical Pacific. The reader is referred to Philander and Seigel (1985) for the background on their experiment and its physical motivation. The hindcasts reported here are carried out as in the Philander and Seigel (1985) experiment, except that a different surface wind stress analysis is used to force each experiment. The ocean circulation model is fully described in Philander and Seigel (1985) and their references. Briefly, it has primitive equation model physics, 27 levels in the vertical (10 evenly spaced in the upper 100 m of the water column), model domain extending from 30°S to 50°N, 0.33° latitudinal and 1.0° longitudinal grid spacing between 10°S and 10°N, horizontal eddy viscosity and heat/salt diffusion, and the Pacanowski and Philander (1980) vertical viscosity and diffusion parameterization. The surface heat flux parameterization assumes constant radiation (longwave and shortwave), but allows sensible and latent heat flux variations; the net flux is assumed to depend only on surface temperature, air–sea temperature difference and wind speed. Section 3 of Philander and Seigel (1985) should be consulted for details of the model and its parameterizations. Initial conditions for all the hindcasts were the same, 15 January from a multiyear integration using Hellerman and Rosenstein (1983) climatological monthly mean wind stresses that was itself started from the Levitus (1982) density field. For completeness and for comparison, the Philander and Seigel (1985) experiment was also repeated and is designated NMC here.

Three ship-of-opportunity XBT lines provide for direct comparison of the model hindcasts with observed ocean variability. The variability of temperature and dynamic height calculated from XBT data is compared with that of the model hindcasts. Section 2 provides a discussion of the changes observed from the XBT data along the tracks. Section 3 provides an overview of the different wind fields, how they were converted to stress fields for these hindcasts, the major changes observed in the fields, and statistics on the differences between the fields. Section 4 provides some discussion of each hindcast, while section 5 presents some statistical hindcast skill results. Section 6 offers a summary and discussion of these hindcast findings and identifies a number of factors affecting hindcast skill.

2. El Niño observed in the ship-of-opportunity XBT dataset

Expendable bathythermographs (XBTs) have been deployed since 1979 from merchant ships operating out of Noumea, New Caledonia under a joint U.S.–France ship-of-opportunity program. The same ships take bucket samples for the determination of surface temperature and salinity. The ships traverse nearly meridional routes in the central and western Pacific and an oblique route between Panama and Tahiti (Fig. 1). The three routes will be referred to as the western Pacific (WP), central Pacific (CP), and eastern Pacific (EP) tracks, and cross the equator at 160°E, 165°W, and 100°W; 5081 XBT profiles have been collected on these routes during 1982–83. These data form the basis for several studies of thermal variability in the

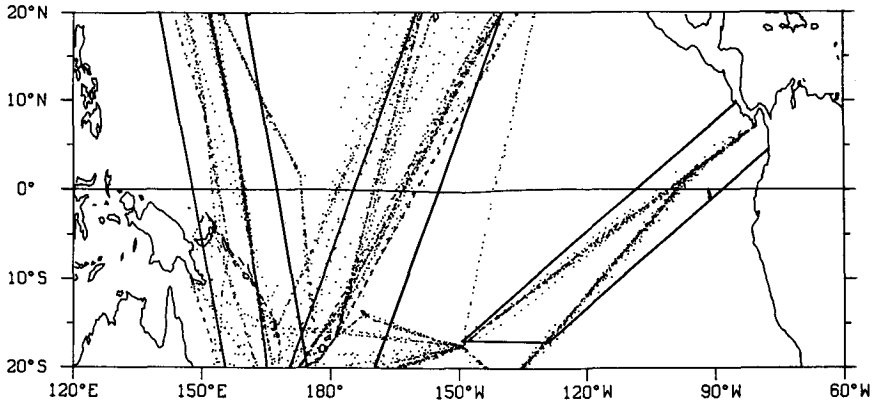

FIG. 1. Geographical scatter of all XBT casts on the ship of opportunity XBT lines for the period 1982–83.

tropical Pacific (Rebert et al. 1985; White et al. 1986; Kessler and Taft 1987). For the purpose of this study any XBT profile taken within 10° longitude of the centerline of each track shown in Fig. 1 was considered to lie on the centerline, and the longitudinal spread of the observations within each track was ignored. (The model hindcasts, on the other hand, were simply sampled exactly on the track centerlines). Approximately two profiles per degree latitude per month were made on each of the three tracks during 1982–83, and the data were bin-averaged with a resolution of one degree latitude and one month. Thus short-period fluctuations such as the 20 to 30-day waves in the eastern equatorial Pacific contribute to aliasing of the monthly data. Kessler and Taft (1987) discuss the gridding process and the errors inherent in the uneven sampling and nonmeridional tracklines.

The three tracks show three distinct thermal regimes during 1982–83; we confine attention to the major events in each region which any successful model hindcast must reproduce. Dynamic height changes provide a convenient basic descriptive variable, and are often found to be the inverse of thermocline depth fluctuations, although significant exceptions to this association will be noted. Dynamic heights were calculated from the XBT temperature profiles and surface salinity observations according to the method of Kessler and Taft (1987), which uses a mean T–S relation below the thermocline but models the mixed layer vertical salinity gradient (starting from the observed surface salinity) to be proportional to the temperature gradient. This method gives an estimate of dynamic height which agrees better with sea level variations measured at oceanic islands than the use of a mean T–S relation alone (Kessler and Taft 1987). In the model hindcasts the salinity field is known, so dynamic heights were calculated directly.

The earliest clear change was a shoaling of the equatorial thermocline on the WP track, where equatorial dynamic height (Fig. 2) fell 8 dyn-cm between February and April 1982. The shoaling extended from 2°S to 7°N in early 1982 (it would ultimately extend from 15°S to 15°N by the end of the year). After a brief rise in July 1982 WP equatorial dynamic height fell 30 dyn-cm in six months. This change was due to a 60 m rise in the thermocline which nearly eliminated the usual 100 m thick upper layer. Despite large thermocline depth anomalies, SST changes were modest; WP equatorial SST fell about 1°C in mid-1982, to about 29°C and remained at this level for about a year (Fig. 3). Surface salinity changed much more than SST, climbing about 0.8‰ between July 1982 and April 1983 (Fig. 4). In January 1983 WP equatorial dynamic height reached its nadir, and through 1983 dynamic height recovered slowly, finishing 1983 about 10 dyn-cm below its level at the beginning of 1982.

On the CP track, equatorial SST gradually warmed from about 27°C in February to about 29°C in July 1982, remained above 29°C until January 1983, and then cooled steadily until October 1983 when it reached about 26°C (Fig. 3). CP equatorial surface salinity was normal until July 1982 and then began rapidly falling: the total decrease of 1‰ by October was to a level typical of pre-Niño conditions in the WP (Fig. 4). Extreme rainfall occurred in the CP but lagged the lowest salinity by two months; peak precipitation occurred in December 1982–January 1983.

Central Pacific thermocline changes began in July–August 1982 with thermocline deepening of about 20 m to more than 100 m depth; the vertical gradient between 28° and 18°C also became very sharp. The 15 dyn-cm rise in CP equatorial dynamic height between July and September 1982 (Fig. 2) resulted largely from the formation of a thick, very low-density upper layer [about half the rise was due to the low salinity alone (Kessler and Taft 1987)], rather than to deepening of the thermocline. A 20 dyn-cm drop then occurred during December 1982 and January 1983 (Fig. 2), due to a rapid 50 m rise in the thermocline. CP dynamic height continued to drop until October 1983,

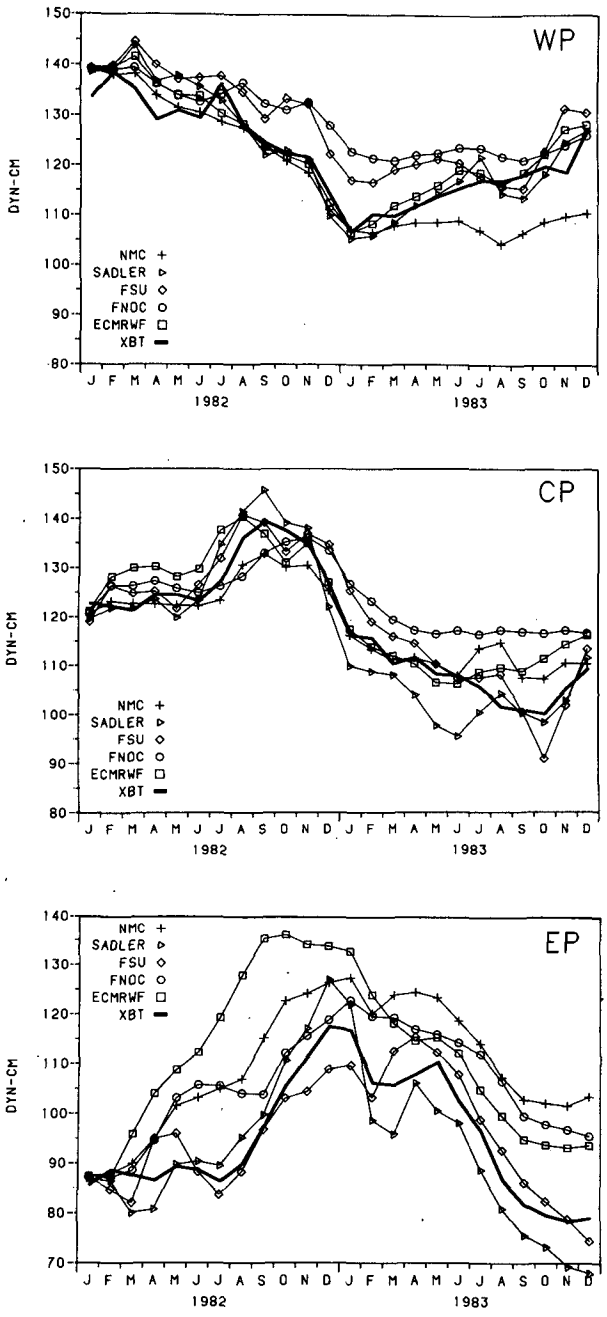

FIG. 2. Dynamic height at the equator on the three ship tracks from the XBT data and model hindcasts. Top panel: western Pacific; middle panel: central Pacific; bottom panel: eastern Pacific.

falling an additional 15 dyn-cm (Fig. 2); much of this resulted from cooling of the upper layer.

Eastern Pacific conditions were normal until August 1982 when the equatorial thermocline began dropping; it then deepened steadily until the end of 1982 by which time the 20°C isotherm was about 80 m deeper and the thermocline sharper than it had been during the previous year (Fig. 5, upper left). SST increased steadily through this same period, from about 24°C to about 28°C, but its maximum (about 29°C) did not occur until April 1983 (Fig. 3). By January 1983 dynamic height on the EP track had risen 30 dyn-cm; note that EP and CP dynamic height were then about the same, and were somewhat higher than in the WP. The warming surface layer accounted for about one-third of the late 1982 dynamic height rise. In February and March 1983 EP equatorial dynamic height fell 12 dyn-cm as

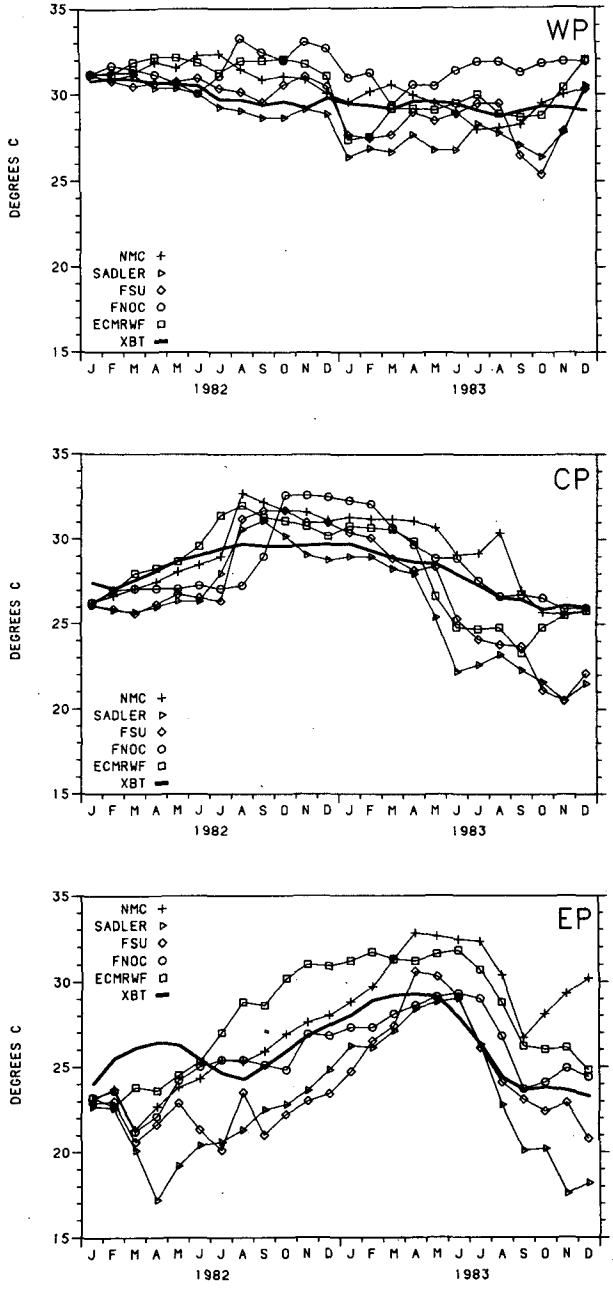

FIG. 3. Sea surface temperature at the equator on the three ship tracks from the XBT data and model hindcasts. Top panel: western Pacific; middle panel: central Pacific; bottom panel: eastern Pacific.

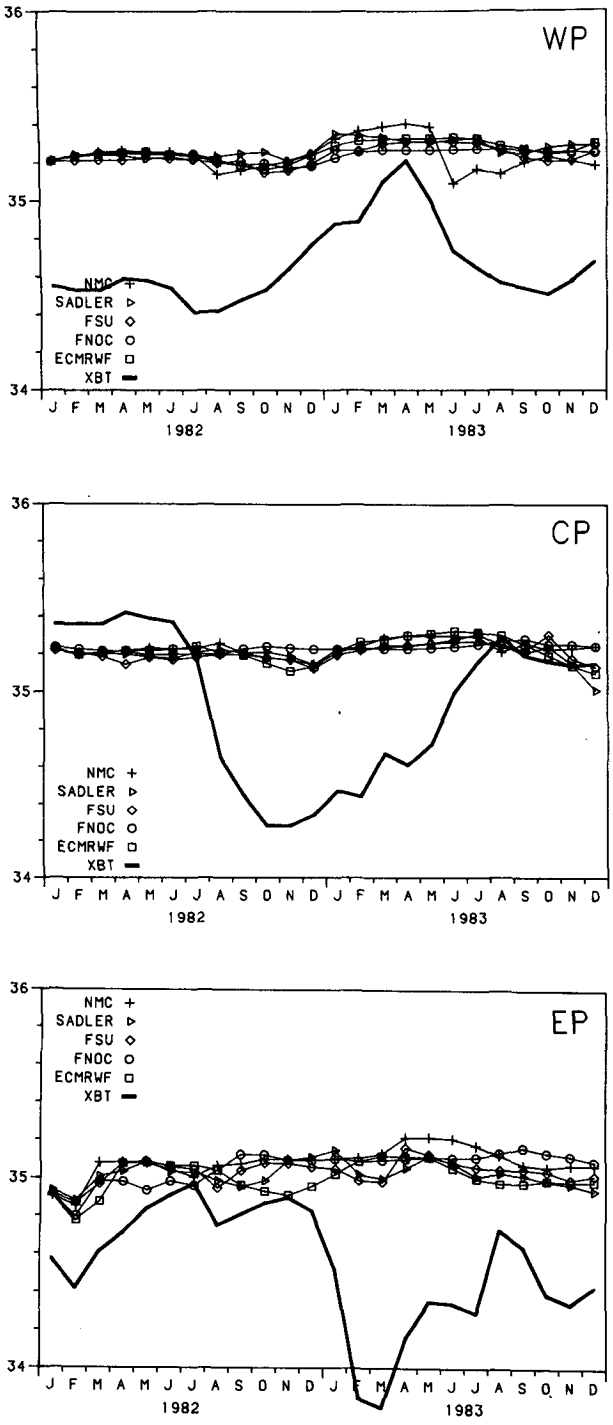

FIG. 4. Sea surface salinity (parts per thousand) at the equator on the three ship tracks from the ship of opportunity data and model hindcasts. Top panel: western Pacific; middle panel: central Pacific; bottom panel: eastern Pacific.

the thermocline recovered partly back to normal levels to a more typical vertical gradient (Fig. 5); in April dynamic height again peaked (Fig. 2). The April 1983 peak resulted from a combination of very near surface warming and from changes in isotherms below 20°C, not from changes in the sharpest region of the thermocline. The 12°C isotherm remained at approximately constant depth at this time, so the deepening of the lower thermocline meant that the usually thick thermostad region of 13°C water contracted to about one-third its normal depth extent (Fig. 5). This dramatic change in stratification, with warming above the main thermocline as well as below it, but with no significant change in the depth of the 20°C isotherm, cannot be described by any roughly equal distribution of amplitude in the first three vertical modes.

During June–November 1983 dynamic height on the EP track fell as the thermocline rose and the warm upper layer disappeared (Fig. 5). In October 1983 dynamic height on all three tracks was 10 to 20 dyn-cm lower than it had been in January 1982 (Fig. 2). The two peaks in dynamic height in the EP (December 1982–January 1983 and April–May 1983) have prompted considerable interest; we shall comment on earlier efforts to explain this aspect of the variability in section 6.

Changes in the thermal structure away from the equator were equally as dramatic as those near the equator, and were associated with large variations in the transport of the major zonal geostrophic currents. On the WP track, dynamic height at 10°N fell 33 dyn-cm between April and November 1982 (Fig. 6). This change, which was larger and peaked earlier than the dynamic height fall on the equator, was due to a 60 m shoaling of the thermocline.

On the CP track, thermocline shoaling also occurred at 10°N in mid- and late 1982, although not quite as strongly as in the WP (Fig. 6). The shoaling was in phase with the usual seasonal shoaling in the CP, and appeared as an exaggeration of the seasonal cycle (Kessler and Taft 1987). The combination of the shallow thermocline ridge near 10°N and the deep warm fresh equatorial upper layer increased the pressure gradient across the CP NECC, and increased NECC surface flow to about 80 cm s^{-1} at 5°N (Fig. 7, upper left). The warm equatorial upper layer in the CP in late 1982 also eliminated the usual equatorial trough in dynamic height which is associated with the westward South Equatorial Current (SEC) spanning the equator (Fig. 7, upper left). No attempt is made to calculate geostrophic currents closer to the equator than 2° latitude, but direct current measurements at 159°W show an eastward equatorial surface jet with speeds up to 140 cm s^{-1} occurred in October to December 1982, replacing the SEC at the equator (Firing et al. 1983).

While in 1982 major anomalies were observed on and north of the equator on the CP and WP tracks, during 1983 the largest changes were south of the equator. Along each track the thermocline shoaled more than 60 m between October 1982 and May 1983 from the equator to 12°S, causing a dynamic height

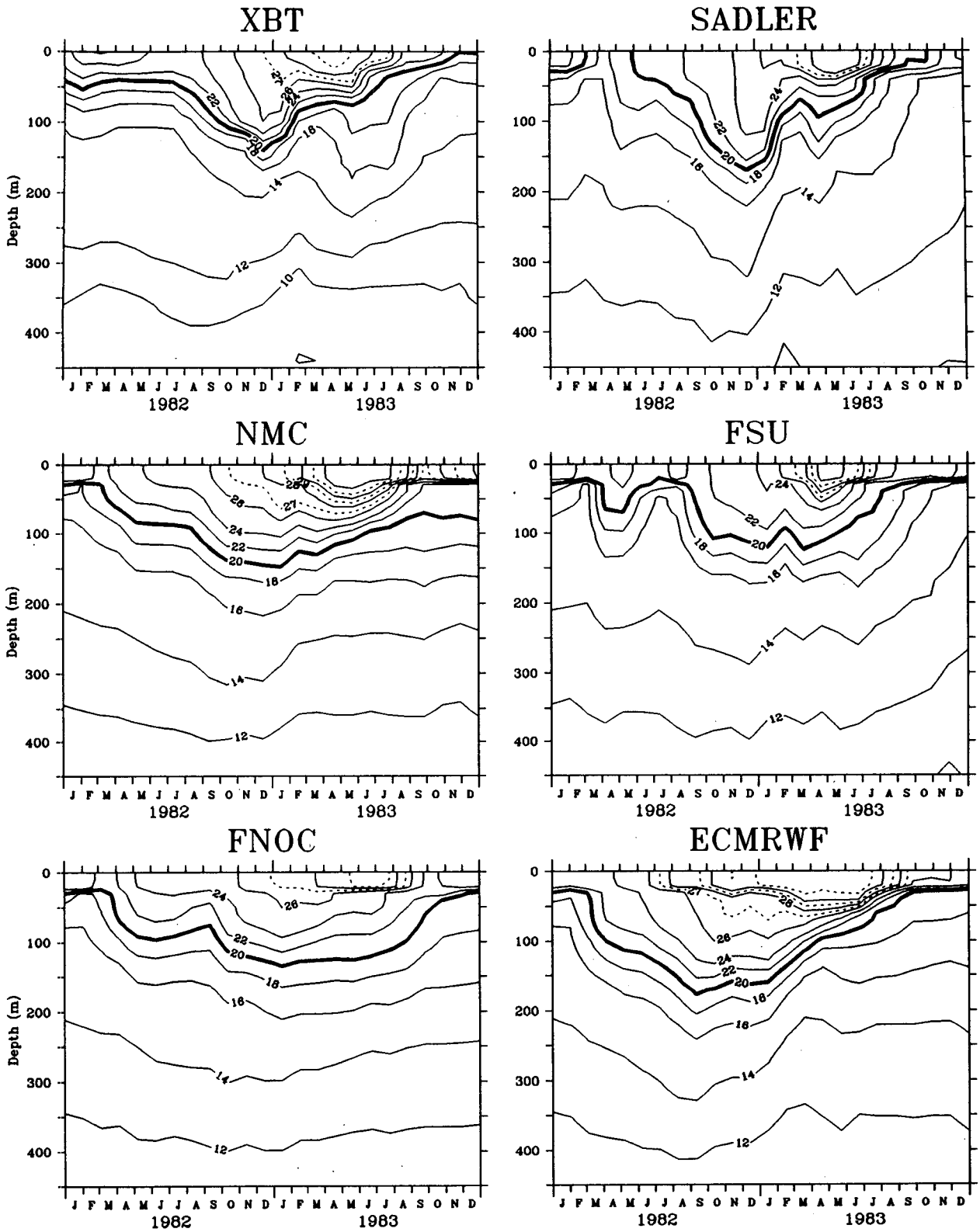

FIG. 5. Temperature at the equator on the eastern Pacific track from the XBT data and model hindcasts.

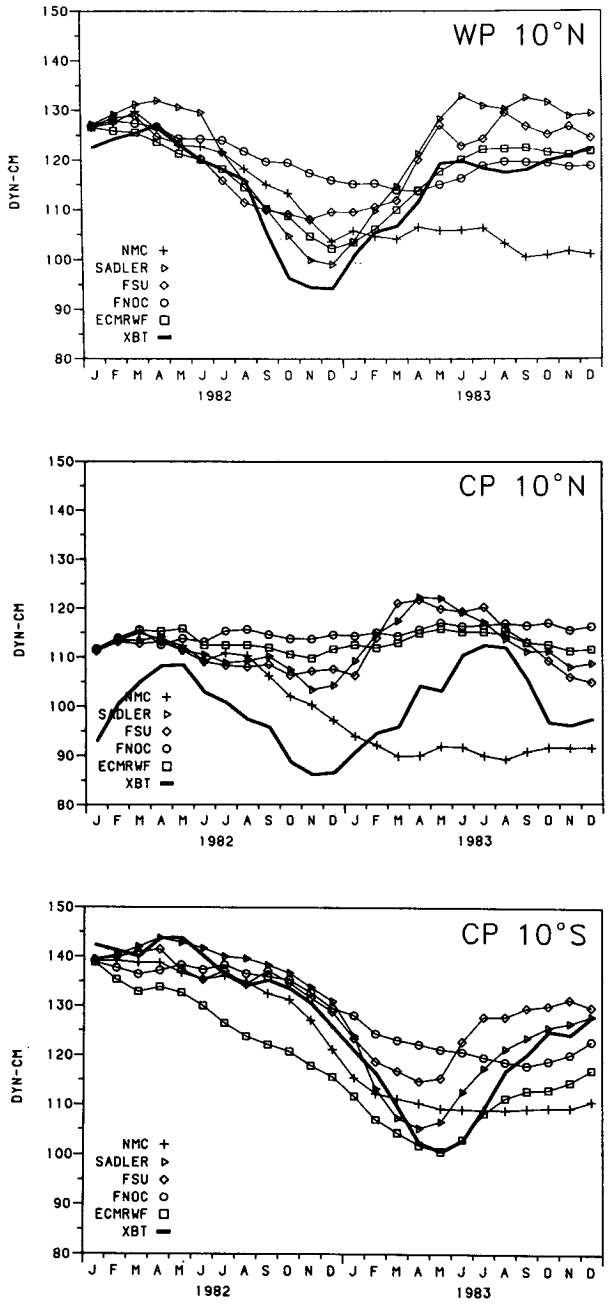

FIG. 6. Dynamic height from the XBT data and model hindcasts. Top panel: 10°N on the western Pacific track; middle panel: 10°N on the central Pacific track; bottom panel: 10°S on the central Pacific track.

drop of more than 40 dyn-cm at 10°S in the CP (Fig. 6). An anomalously strong South Equatorial Countercurrent was seen between January 1983 and June 1983 in the range 3° to 8°S.

The shoaling of the thermocline in the Southern Hemisphere occurred nearly simultaneously with the equatorial shoaling, resulting in an uplifted thermocline and low dynamic heights stretching across the equator from 5°N to 12°S in both regions during mid-1983. At 10°N dynamic heights rose in midyear in accordance with the usual annual cycle (Kessler and Taft 1987), and the combination of the seasonally high 10°N dynamic height and the abnormally low equatorial dynamic height nearly eliminated the usual pressure gradient across the NECC; it recovered as conditions became more normal later in 1983 (Fig. 7).

3. The wind stress fields

The momentum flux (wind stress) at the ocean surface must be specified for the hindcasts to be carried out; a number of different analyses are available for 1982–83. Three sets of monthly mean surface stress fields were produced from operational meteorological center products: by N. Wells (personal communication 1985), using data from the European Centre for Medium Range Weather Forecasting (ECMWRF), by Philander and Seigel (1985), using the 1000 mb winds from the National Meteorological Center (NMC) and by us, using six-hourly nominal 10 m height winds from the Fleet Numerical Ocean Central (FNOC) (their A-29 and A-30 surface marine wind products). Monthly mean pseudostress analyses were produced by Florida State University (FSU) from surface data (Goldenberg and O'Brien 1981) and by J. Sadler (SADLER) from low-level cloud motion vectors, a climatological wind shear field between the surface and cloud level, and surface observations (Sadler and Kilonsky 1985). The pseudostress fields must be multiplied by air density times drag coefficient (C_d) to obtain stress values.

The FNOC wind data were converted to stress fields using the C_d formulation of Large and Pond (1981) and assuming relative humidity of 0.75 and climatological air–sea temperature differences; these stresses were then monthly averaged. Two FSU stress fields were made from the FSU pseudostress fields—using $C_d = 1.2 \times 10^{-3}$ and $C_d = 1.5 \times 10^{-3}$—for separate experiments. Here 1.2×10^{-3} is a reasonable value for winds of roughly 5 m s^{-1} under typical central tropical Pacific conditions according to Large and Pond (1981), while 1.5×10^{-3} is the value used by Wyrtki and Meyers (1975) and is typical of the Bunker (1976) C_d formulation for these conditions. In most respects the weaker stress field gave better results than the stronger field; results denoted FSU pertain to the weaker stress fields. The Sadler (SADLER) stress fields were made from the Sadler pseudostress fields using $C_d = 1.2 \times 10^{-3}$. We used constant C_d values to convert pseudostress fields to stress fields because, lacking information on the high frequency variability within each month, this is the most straightforward approach.

These fields provide the forcing data for the hindcasts to be discussed here. Although a detailed discussion of the differences between the different stress fields will not be given, it is useful to consider certain common

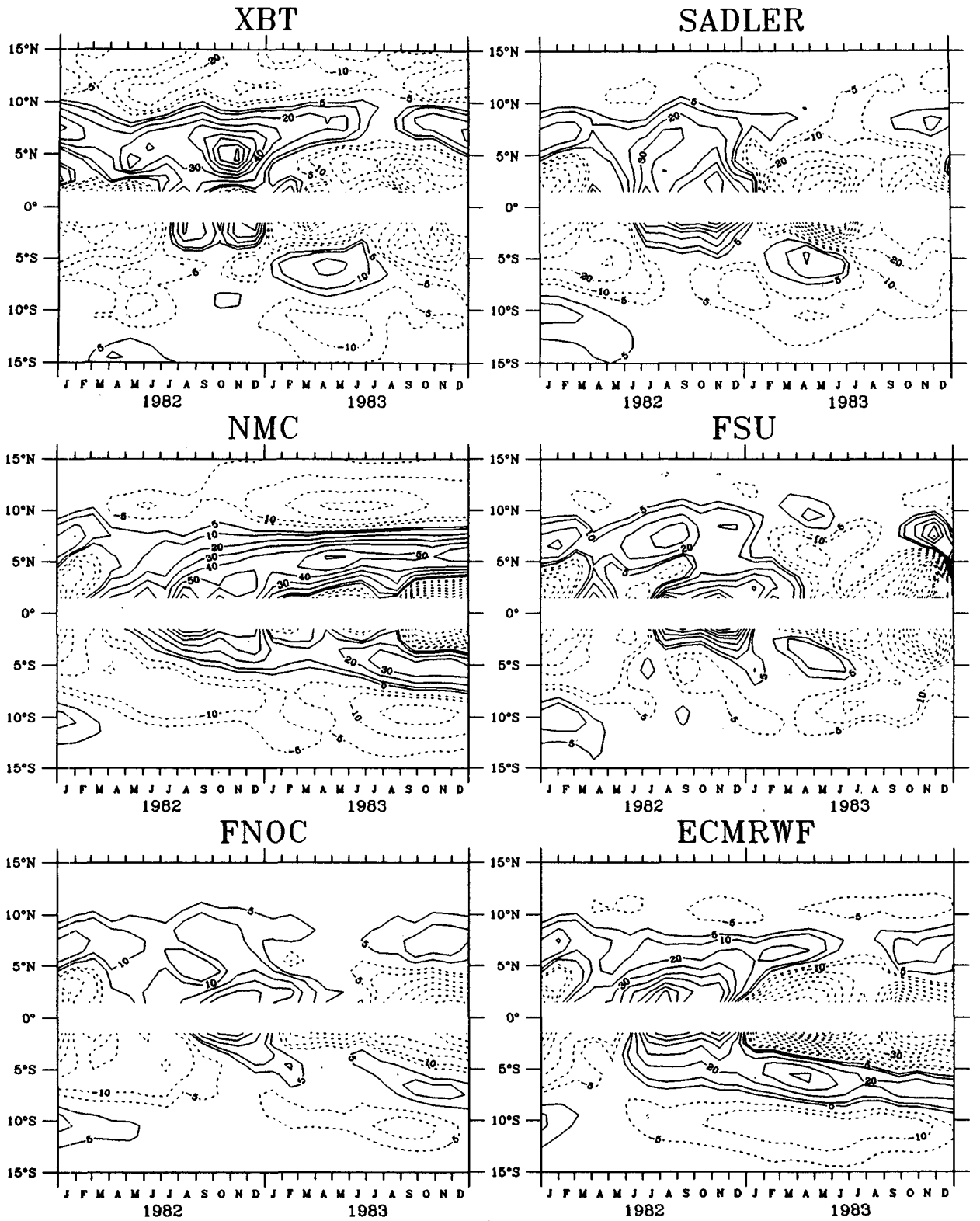

FIG. 7. Surface zonal geostrophic speed (cm s^{-1}) relative to 450 m on the central Pacific track from the XBT data and model hindcasts.

elements of the fields and the major differences between them. Before examining specifics along the different ship tracks, some general comparisons can be offered. Overall there is considerable qualitative similarity between the different stress fields. The FSU and SADLER fields are generally the most similar, not surprisingly along the ship tracks, as they both depend heavily upon ship wind observations, but the FSU fields generally possess more spatial variability in a given month and greater month-to-month variability in a given location. FSU amplitudes are typically 20% smaller than SADLER amplitudes. Although FNOC also makes heavy use of ship observations, the results of the stress calculation here produced fields both much weaker in amplitude than FSU and sometimes quite different in spatial structure from FSU and SADLER. The ECMRWF and NMC fields tend to exhibit the least spatial structure, not surprisingly as they are produced on grids with the coarsest meridional resolution of any of the fields.

Figure 8 shows the vector stress time series according to SADLER, and offers one version of the major wind changes that took place during 1982–83. We show the SADLER fields because the changes are large enough to be seen easily, because there is often qualitative similarity to the other fields, and because good hindcast results for dynamic height variability were frequently obtained with the SADLER fields. The Hellerman and Rosenstein (1983) climatological stress fields are also shown in Fig. 8 for reference; recall that these were the wind stresses used in the model spinup to the initial state for these hindcasts.

In the western Pacific (Fig. 8, top panels) the normal regime prevailed early in 1982, with the (boreal) winter monsoon pattern in evidence; the austral summer northwesterly monsoon between 5° and 15°S was stronger than climatology in January 1982. In March 1982 there was westerly stress on and just south of the equator, when climatologically the western Pacific easterlies are at their seasonal maximum. The usual Southern Hemisphere (SE) trades began to build in May 1982, but unusually intense southerly flow appeared in the Southern Hemisphere in June/July, while westerly stress extended from about 2°S to as far as 10°N (Harrison 1984). The anomalous westerly flows continued for at least several months. The NE Trades returned abruptly in December 1982, and brought unusually strong northerly cross-equatorial flow that persisted for several months; during the first months of 1983 there was also strong westerly stress between about 5° and 12°S. The SE trades reformed in mid-1983, with somewhat greater than usual strength near 5°S.

Along the central Pacific track (Fig. 8, middle panels) the prevailing trade wind regime was less visibly disrupted, except between September 1982 and April 1983. The usual waveguide easterlies were replaced by calm conditions in September 1982. Weak westerly stress began on and just north of the equator in October. In November westerly stress reached 0.4 dyn cm^{-2} centered on the equator; thereafter westerlies were only found south of the equator. Between January and March 1983, winds were similar to those seen on the western track, with northerlies extending across the equator and westerlies between 5° and 10°S; of course these represent much larger anomalies than in the WP. Normal conditions returned by May 1983 on the equator. The core of the SE trades (roughly 10°S) was stronger than usual in June–July 1983.

Along the eastern Pacific track (Fig. 8, lower panels) the departures from climatology tended to be isolated to a few particular months of weaker or stronger than normal prevailing conditions. The only clear period of unusual conditions was March–April 1983, when the winds tended to be unusually light.

Those interested in how the different wind fields compare in detail should consult the Technical Data Memo by the authors (HKG 1988), which presents a variety of figures describing the different wind fields and their statistics. Here we offer Fig. 9, which shows the different zonal wind stress fields along the equator for the three tracks, with the Hellerman and Rosenstein (1983) climatology for comparison. Many qualitative similarities exist between the analyses: predominantly westerly stress from July through November 1982, followed by an abrupt return to easterly stress in December 1982 in the WP, predominantly westerly stress in October–December 1982, followed by a return to easterly stress in January 1983 in the CP, and very small stress in May–June 1983 in EP. But there are also qualitative differences of note: the early occurrence of westerlies in 1982 in the CP (ECMRWF compared to the others), the sharp drop in easterly stress in the CP in October 1982 in SADLER. FSU and FNOC compared to a small decrease (NMC) or (oppositely) a reduction in westerly stress (ECMRWF), the very weak stress that persists through the middle of 1983 in NMC and FNOC compared with the return of substantial easterlies in the others, etc. HKG (1988) reveals that differences of 0.2–0.3 dyn cm^{-2} are common, and that differences of 0.5 dyn cm^{-2} are not unusual; our knowledge of the monthly surface stress variations in the tropical Pacific remains uncomfortably limited.

4. El Niño in the model runs

a. Common features

The model runs as a group did reasonably well in hindcasting many of the large-scale features of the El Niño within 2 or 3 degrees of the equator, in particular the dynamic height field. Correlation of near-equatorial 0/450 m dynamic height (Fig. 2 and section 5) of all the models with the XBT observations was above 0.9 on the WP and CP tracks and above 0.8 on the EP track. All the hindcasts showed the year-long fall of equatorial dynamic height in the WP during 1982 (Fig. 2). In the CP, all the runs displayed an increase of

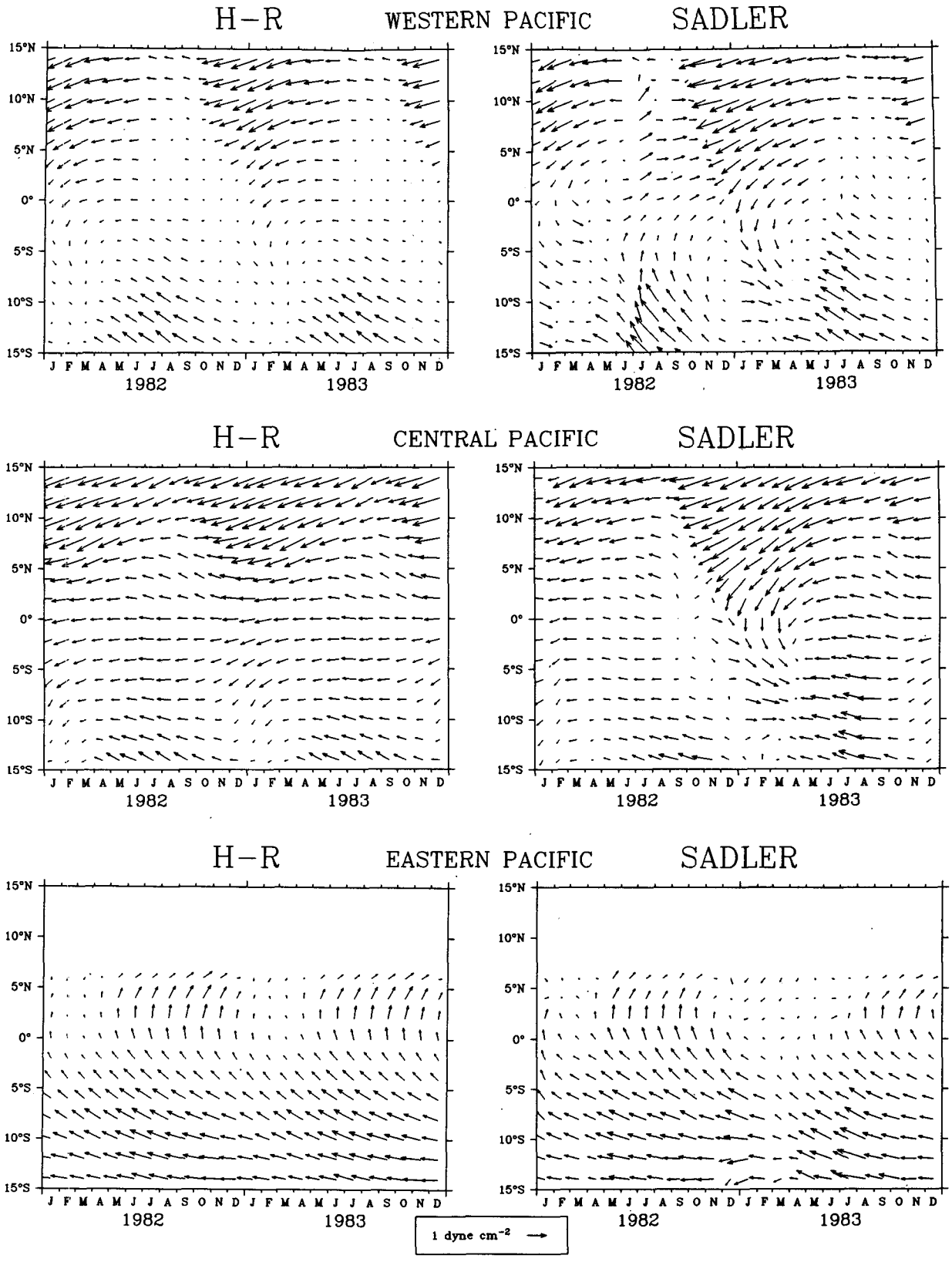

FIG. 8. Monthly mean surface wind stress vectors on the three ship tracks from the Hellerman and Rosenstein (1983) climatology and the Sadler wind analysis. Left panels: Hellerman and Rosenstein; right panels: Sadler. Top panels: western Pacific; middle panels: central Pacific; bottom panels: eastern Pacific. The scale vector at bottom center indicates 1 dyn cm^{-2}.

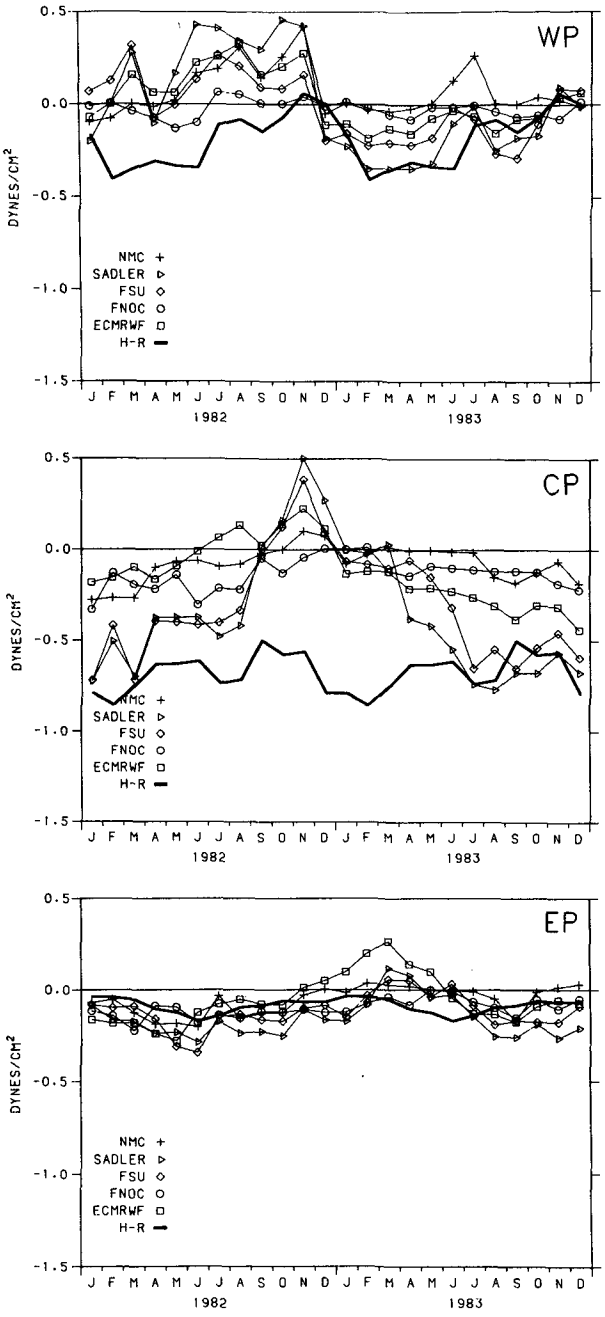

FIG. 9. Zonal component of the wind stress (τ^x) at the equator on the three ship tracks from the Hellerman and Rosenstein (1983) climatology and the five wind products studied. Top panel: western Pacific; middle panel: central Pacific; bottom panel: eastern Pacific.

equatorial dynamic height and SST in late 1982 and a sharp fall during 1983, as was observed (Fig. 2). Associated with these dynamic height events spanning the equator were large changes in the zonal geostrophic currents (Fig. 7), (which were computed by differencing the dynamic height fields in the regions poleward of 2° latitude). In both the CP and WP, the hindcasts all showed an increase in eastward geostrophic flow north and south of the equator in late 1982, similar to observations. In 1983 in the CP, all the runs reproduced the strong westward SEC spanning the equator, and all except the NMC run showed the near-disappearance of the NECC in mid-1983, with westward flow extending to 6°–7°N as observed. In the EP, dynamic heights on the equator were more scattered about the data than on the other two tracks, but the phases of the fluctuations were quite similar for most of the runs (Fig. 2). The double peak of dynamic height was evident to some degree in all but one case (ECMRWF), however the vertical temperature variations responsible for these peaks were usually not well reproduced (Fig. 5).

Some discrepancies with the observations common to all the model runs are due to model ocean conditions at the beginning of the hindcast in January 1982, following several years of spinup with climatological stresses. From the zonal geostrophic speeds (Fig. 7) we see that: the model North Equatorial Current (NEC) was only about one-quarter as strong as observed; the South Equatorial Countercurrent (SECC) was relatively strong (about 10 cm s^{-1}) near 10°S in the WP and CP [which is in accord with observations of a normal year in the XBT data, but was not the case at the beginning of 1982 in the CP (Kessler and Taft 1987)]; the model NECC was slightly weaker than observed in the XBT data in January 1982 on the CP track. The initial surface salinity field contained much weaker gradients than were observed.

Surface temperature was not well hindcast quantitatively in any of the model runs. Hindcast SST variability (Fig. 3 and HKG 1988) was considerably larger in almost every location than observed; the model developed unrealistically high maximum temperatures in the weak wind stress hindcasts, and unrealistically low minimum temperatures in the cold tongue in the strong wind stress hindcasts.

Large wind stress changes outside the equatorial waveguide generally do not lead to rapid, easily interpreted ocean changes. One exception occurs if simple Ekman pumping physics is strongly at work, by which we mean that the change in the depth of an isotherm (here we shall use 20°C) is related to the curl of the wind stress through

$$-\partial h/\partial t = \mathrm{curl}_z(\tau/\rho f), \qquad (4.1)$$

where h is the depth of the 20°C isotherm (positive down), τ the wind stress, ρ the density of seawater and f the Coriolis parameter. We have computed correlations between the two terms in (4.1) to assess the degree to which such a simple balance exists in the hindcasts. Figure 10 summarizes these calculations; specific results will be discussed below.

b. NMC hindcast

The NMC hindcast, which has previously been discussed by Philander and Seigel (1985) and has some

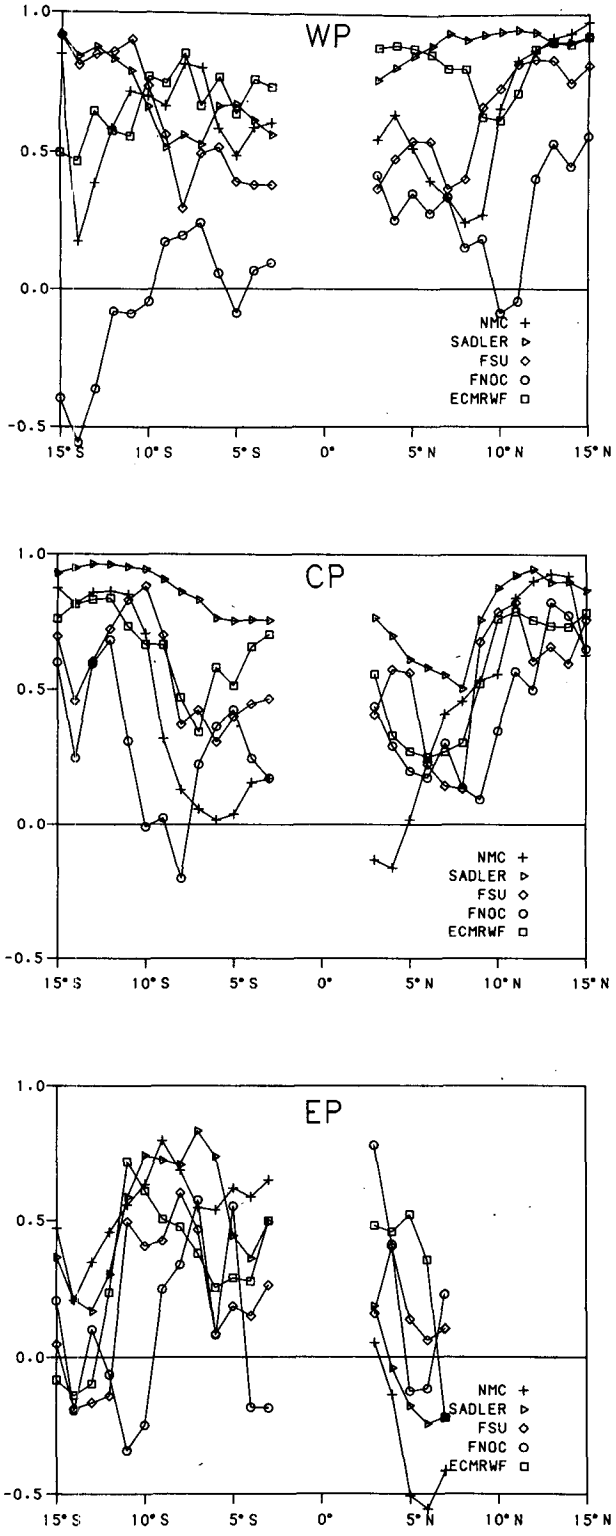

FIG. 10. Correlation of the Ekman pumping balance on the three ship tracks from the five model hindcasts. In each case $\partial h/\partial t$ is estimated from monthly changes in the depth of the 20°C isotherm, and curl$(\tau/\rho f)$ is found from the corresponding wind product. Top panel: western Pacific; middle panel: central Pacific; bottom panel: eastern Pacific.

important correspondences with observations, is also the only one to exhibit large scale behavior grossly inconsistent with observations (its NECC in 1983).

In the WP on the equator, NMC dynamic height fell similarly to the observations during 1982, but never recovered during 1983, so by the end of the hindcast period NMC dynamic heights were about 15 dyn-cm lower than those observed in the XBT data and all the other model runs (Fig. 2). On the EP track, on the other hand, NMC dynamic height ended the hindcast period with equatorial dynamic height about 25 dyn-cm higher than observed (Fig. 2). Thus the zonal dynamic height difference across the basin at the end of 1983 was only 6 dyn-cm in the NMC hindcast, compared to 48 dyn-cm in the XBT data and 27 to 60 dyn-cm in the other model runs. NMC wind stress on the equator never rose much above 0.2 dyn cm^{-2} anywhere and averaged near zero on all three tracks, compared to the seasonal winds which averaged 0.6 dyn cm^{-2} in the CP (see section 3).

The hindcast vertical profile of equatorial temperature on the EP track (Fig. 5) was similar to the XBT profile during 1982, but differed strongly during 1983. The observations show downward isotherm motion in the lower thermocline during February to June 1983, while NMC shows a steady upward trend. The second peak in dynamic height in the NMC EP hindcast (Fig. 2) is due primarily to the very high upper layer temperature (SST greater than 32°C), rather than to thermocline variations as in the XBT observations.

The hindcast NECC in the CP and WP strengthened in late 1982 as in the observations, but then continued to strengthen during 1983 while the observed NECC (and the NECC in all the other runs) nearly disappeared (Fig. 7). At 10°N in the CP and WP (near the northern boundary of the NECC), NMC dynamic heights never recovered from the late 1982 drop and remained about 20 dyn-cm below those observed (Fig. 6); consequently a large pressure gradient drove the unrealistic NMC NECC during 1983. In the NMC wind field a sharp gradient existed between strong NE trades and continuing near-zero stress spanning the equator in late 1982–early 1983 (HKG 1988). The strong (Ekman upwelling) curl associated with this meridional gradient of zonal wind stress apparently kept the model thermocline rising (see Fig. 10; correlation greater than 0.8 poleward of 10°N on CP and WP) to extremely high levels, producing low dynamic height at 10°N and a strong NECC, out of phase with the observations.

In the Southern Hemisphere NMC CP, dynamic height fell at the end of 1982 (as in the data) but did not recover in the last half of 1983 as was observed (Fig. 6). The drop in Southern Hemisphere dynamic height in late 1982 was in phase with the local Ekman pumping (correlation > 0.8 in the CP, from 11° to 18°S), as was the lack of a recovery in 1983. As noted above, in mid-1983 the NMC winds were very weak near the equator; together with significant easterlies

well south of the equator, enough wind stress curl existed to produce upwelling from the equator to 15°S. The resulting fall of dynamic height near 10°S led to the development of eastward geostrophic flow (a SECC) early in 1983 as in the XBT observations but, unlike the observations, the model eastward flow persisted and strengthened through 1983 (Fig. 7). The meridional profile of zonal geostrophic flow was quite symmetric about the equator in mid-1983, with net transport between 10°S and 10°N strongly eastward, while the XBT observations show net westward geostrophic flow in the same region (Fig. 7).

c. *SADLER hindcast*

The SADLER hindcast consistently gave among the best simulations of observed dynamic heights; correlations exceeded 0.9 from 15°S to 16°N on the WP track, from 18°S to 4°N on the CP track, and from 5°S to 6°N on the EP track, and rms differences from the data were generally among the smallest (see Figs. 2, 6 and HKG 1988). The double peaks in the eastern Pacific were best reproduced in this hindcast; it was the only one to produce a large second peak which was stronger in the lower thermocline than at 22° to 26°C (Fig. 5). Near 10°S on the CP track, where the thermocline uplift caused the largest dynamic height fluctuation observed in the entire XBT dataset (in early 1983), only the SADLER hindcast reproduced the amplitude (Fig. 6). (Note that the Ekman pumping balance held very well (correlations > 0.95) in the CP and WP between 10° to 15°N and 10° to 15°S, where the comparison with observations is good).

It must be noted that the dynamic height results were not everywhere consistent with observations. The NECC was too weak through much of the period, in some areas by as much as a factor of 2, and in mid-1983, when the observed NECC was very weak but still present, the SADLER NECC region showed weakly westward flow (Fig. 7).

This hindcast consistently produced the lowest SST values of any of the model runs. While never developing the extremely high equatorial temperatures found in many of the other hindcasts, equatorial SST was underestimated by about 2°C during 1983 on the WP track, by about 5°C during late 1983 on the CP track, and by 2° to 5°C during the entire period on the EP track (Fig. 3).

d. *FSU hindcast*

The FSU hindcast had a number of similarities to the SADLER run but, because the FSU wind stress product contained more variance in small space and time scales (see section 3), was significantly noisier and generally had lower correlations with the observations (see HKG 1988). Like SADLER, the FSU hindcast a NECC peak in late 1982 and produced a complete cessation of the NECC in mid-1983 (Fig. 7). FSU and SADLER were the only hindcasts which showed the observed event of eastward flow near 5°S in the CP in early 1983 which later disappeared (Fig. 7); the others tended to show this flow continuing through 1983.

The FSU off-equatorial behavior was generally less dominated by Ekman pumping than was SADLER, with a weaker and less consistent correlation between the terms of the Ekman pumping balance (Fig. 10).

Like SADLER, the FSU run also tended to hindcast low waveguide SST (Fig. 3). In the EP, FSU produced a weak first peak of dynamic height and a stronger second peak, unlike the observations (Fig. 2). These peaks were associated with two very similar thermocline downwelling events, both involving the entire thermocline, unlike the observations; the second peak of dynamic height was higher than the first because of high temperatures in a relatively deep upper layer during March to May 1983 (Fig. 5).

e. *ECMRWF hindcast*

The ECMRWF experiment produced the best hindcast of the 1983 disappearance of the NECC, in terms of surface geostrophic zonal current, in 1983. Westward geostrophic flow spanning the equator was hindcast on the CP and WP tracks in 1983, as in the observations, but speeds in the hindcast were higher (Fig. 7). A significant departure from observations was the strong eastward flow near 5°S in the CP persisting through 1983. This flow was associated with dynamic height near 10°S remaining low, instead of recovering as observed (Fig. 6).

In the EP, the model hindcast a much larger and earlier equatorial dynamic height peak than was observed in the XBT data or any of the other model runs (Fig. 2); this was due to the thermocline deepening and upper-layer warming which occurred much earlier than in the observations or the other hindcasts (Figs. 5 and 3). Possibly the early appearance of warm water in the EP was related to the earlier weakening of the ECMRWF trades on the equator in the CP (Fig. 9).

Correlations between the terms of the Ekman pumping balance were more scattered than in the SADLER hindcast, however high correlations were found poleward of about 10°N in the CP and WP and within about 7° of the equator in the WP (Fig. 10).

f. *FNOC hindcast*

The FNOC wind stresses (produced by us from FNOC winds) were consistently the weakest of the five wind products studied (see section 3), so dynamic height variance was also often smallest, particularly in the CP and WP (Figs. 2 and 6). In addition, zonal geostrophic currents were weaker than in any of the other model runs (Fig. 7). The FNOC hindcast had

the highest average SST in the WP, but produced one of the best hindcasts of EP equatorial SST. On the equator in the eastern Pacific there was practically no change in the vertical temperature gradient structure (Fig. 5); unlike the other hindcasts or the observations, the FNOC thermocline slowly rose and fell while the vertical temperature gradient stayed relatively constant. Ekman pumping appeared to have little effect on the FNOC model ocean, except possibly at the far northern end of the CP track (Fig. 10).

5. Hindcast skill statistics

We have thus far provided largely anecdotal comparisons of the data and hindcast results. However a great number of comparison statistics (rms variability, rms differences between hindcast and observations, correlations, EOFs, etc.) have been evaluated, and are presented in HKG (1988). The statistics emphasize that there is no overall "best" hindcast, although particular hindcasts can be best for a particular variable or a particular aspect of 1982–83 behavior. Faced with no simple way to summarize all the comparison statistics, we shall present some measures of hindcast skill to offer quantitative perspective on the hindcast successes and shortcomings.

The skill measure we shall use is

$$S = \frac{\text{rms variability in the XBT record}}{\text{rms difference between the hindcast and XBT data}}.$$

Basically S is a signal-to-noise ratio so one hopes to find large values of S, indicating that the difference between the hindcast and data is much smaller than the signal in the data. We find that when $S > 2$ the correlation between hindcast and observations always exceeds 0.9, which is above the 99% confidence level (for four degrees of freedom, which we take to be appropriate for most of the thermal statistics presented here, based on examination of autocorrelation functions). We also found no instance in which the correlation between hindcast and data was greater than 0.7 (which cannot be distinguished from zero with four degrees of freedom) when $S < 1$. For these reasons, we find it useful to define quantitative hindcast skill to correspond with $S > 1.5$, to define marginal hindcast skill to correspond with S roughly unity, and to speak of qualitative hindcast skill when $S < 1$ but there is positive correlation between hindcast and data.

There are several ways the denominator of S could be evaluated. We have made calculations in two ways, the first in which the 1982–83 means for the data and the hindcast are removed before computing the rms difference, and the second in which the difference existing at the beginning of the hindcast is removed. Because the ocean model could not be initialized with January 1982 conditions, there are some nontrivial differences at this time. The second approach is more demanding of model performance; in the EP, skill scores for NMC, ECMWF and FNOC for subsurface thermal variations drop to qualitative skill from nearly quantitative skill. We shall present skill results based on the second approach.

We have also made skill calculations for the 18-month period, January 1982–July 1983, because this period includes the major ocean variations of the ENSO event; in the NMC hindcast, where there was poor performance in the latter half of 1983, changing the interval of interest can improve skill scores to a level of marginal skill. But generally no significant skill increases or decreases result from such a change.

Figure 11 presents the 1982–83 mean XBT temperature fields along each track, as well as the 1982–83 standard deviations along each track; these are useful for interpreting the skill plots. Note that the largest standard deviations are 3–4°C along each track and occur in the thermocline. SST standard deviations are considerably less, and maxima are found in the equatorial waveguide and near 10°N. The hindcast standard deviations for SST and thermocline temperature tend to be comparable [HKG (1988)]. Because the data standard deviations become so small below the thermocline, extremely accurate hindcasts would be required to produce quantitative hindcast skill.

Eastern Pacific temperature skill results are presented in Figure 12. Quantitative hindcast skill is found in the waveguide in the FSU and SADLER hindcasts, with maximum values [about 2 (FSU) and 3 (SADLER)] in the thermocline. There is a very small area of $S > 1.5$ in NMC, at about 50 m depth between 3° and 5°N, but otherwise it exhibits at best marginal skill, as do ECMWF and FNOC. Subthermocline skill varies greatly with location and hindcast. Waveguide SST skill varies from about 0.4 to a bit less than unity; basically only qualitative hindcast skill exists for SST.

Central Pacific temperature hindcast skill is presented in Fig. 13. Two patterns of hindcast skill are found. FSU, SADLER and FNOC have a band of quantitative skill in the thermocline extending from about 7 or 8°S into the waveguide, while ECMWF and NMC have two regions of quantitative skill, one centered near 10°S and the other in the waveguide; maximum skill is a bit greater than 2. SADLER, FSU and ECMWF also have a small region of marginal skill in the thermocline near 10°N. NMC has conspicuously low skill (about 0.4) in the NECC region, because of its incorrect phasing of 1983 variability.

Western Pacific temperature skill is shown in Figure 14. The patterns of marginal and quantitative hindcast skill are rather variable between hindcasts, and maximum skill is generally not found in the equatorial thermocline. Rather than list the differences, the reader should browse Fig. 14; maximum skill remains about 2 (in FSU, NMC and SADLER) and is found near 7°S in the thermocline. SST skill remains typically

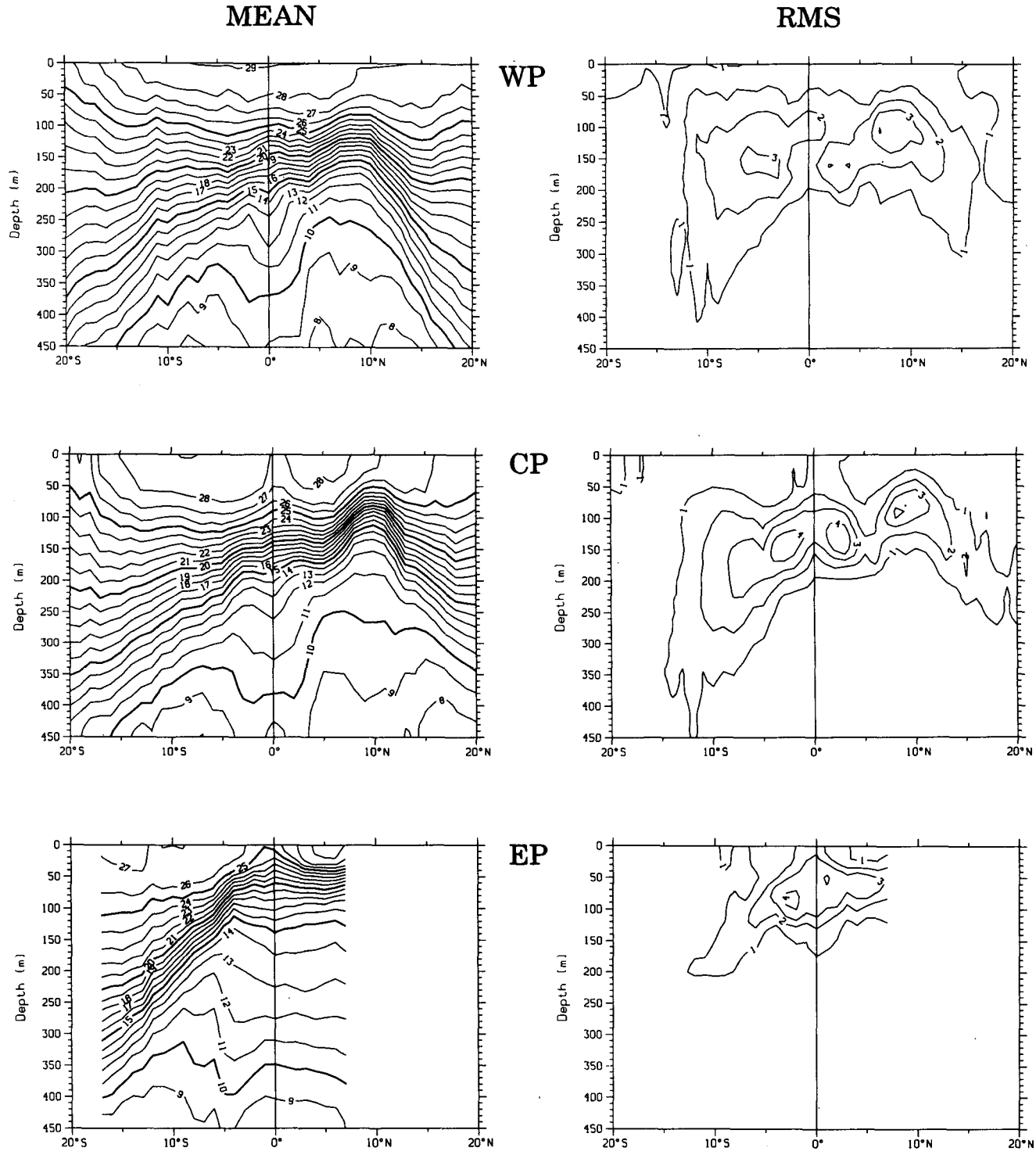

FIG. 11. Observed mean (left panel) and rms (right panels) XBT temperature (degrees C) during 1982–83 along the three XBT tracks. Top panels: western Pacific; middle panels: central Pacific; bottom panels: eastern Pacific.

about 0.4. NMC skill in the NECC region is lowest (about 0.4), while some hindcasts have at least marginal skill there.

The 0–450 m dynamic height skill results are shown in Fig. 15. In the EP, only SADLER and FSU have quantitative hindcast skill over a significant band of

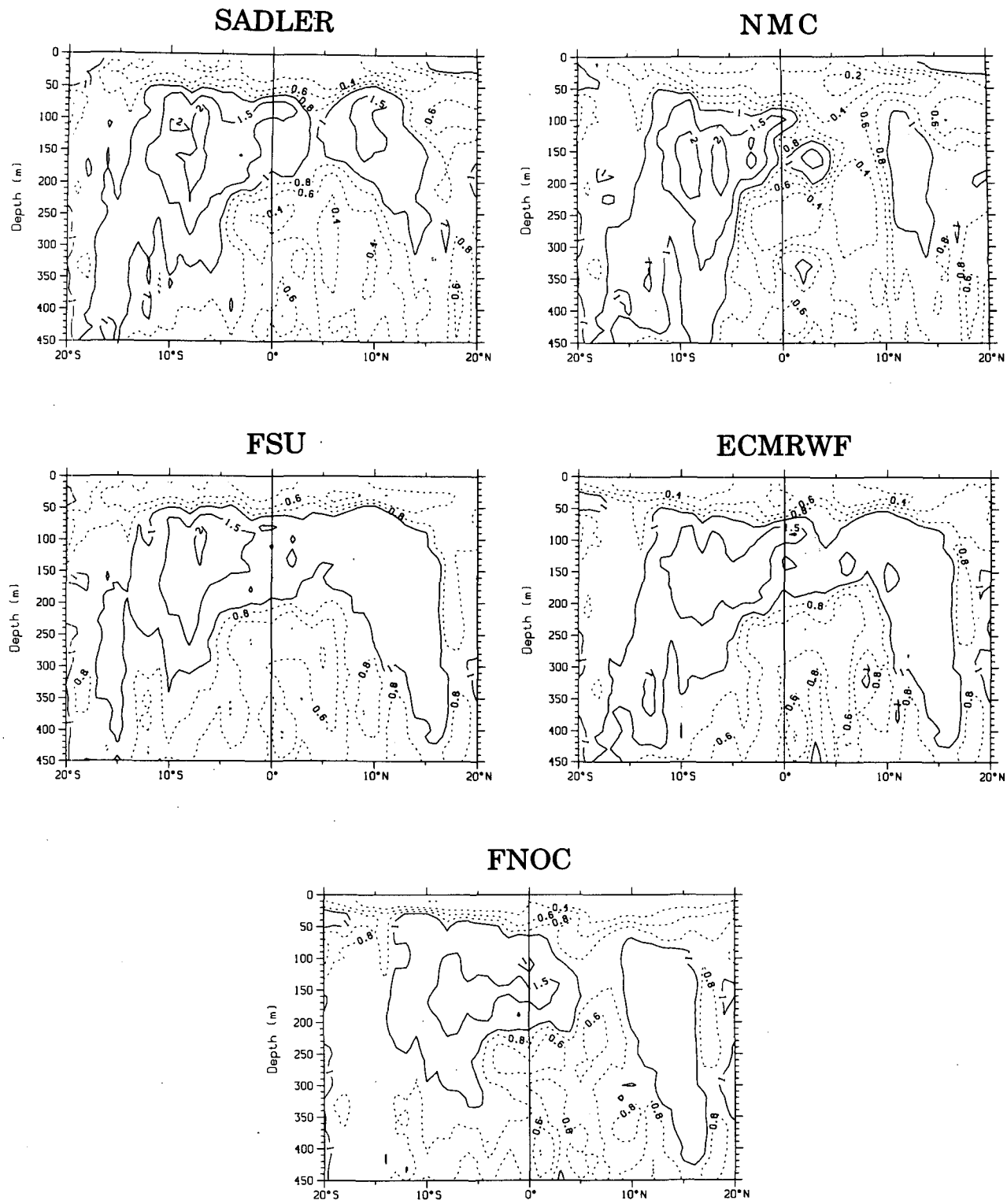

FIG. 12. Hindcast skill index for temperature on the western Pacific track from the five model hindcasts (see text).

latitude; SADLER over the latitude range 2°S to 6°N and FSU between 1° and 7°N. Marginal hindcast skill is found for FNOC and NMC between 3° and 7°N and near 15°S; ECMWF also has skill near 15°S. In the CP, skill is generally higher; between 3°N and 10°S there is at least marginal skill for each hindcast, and

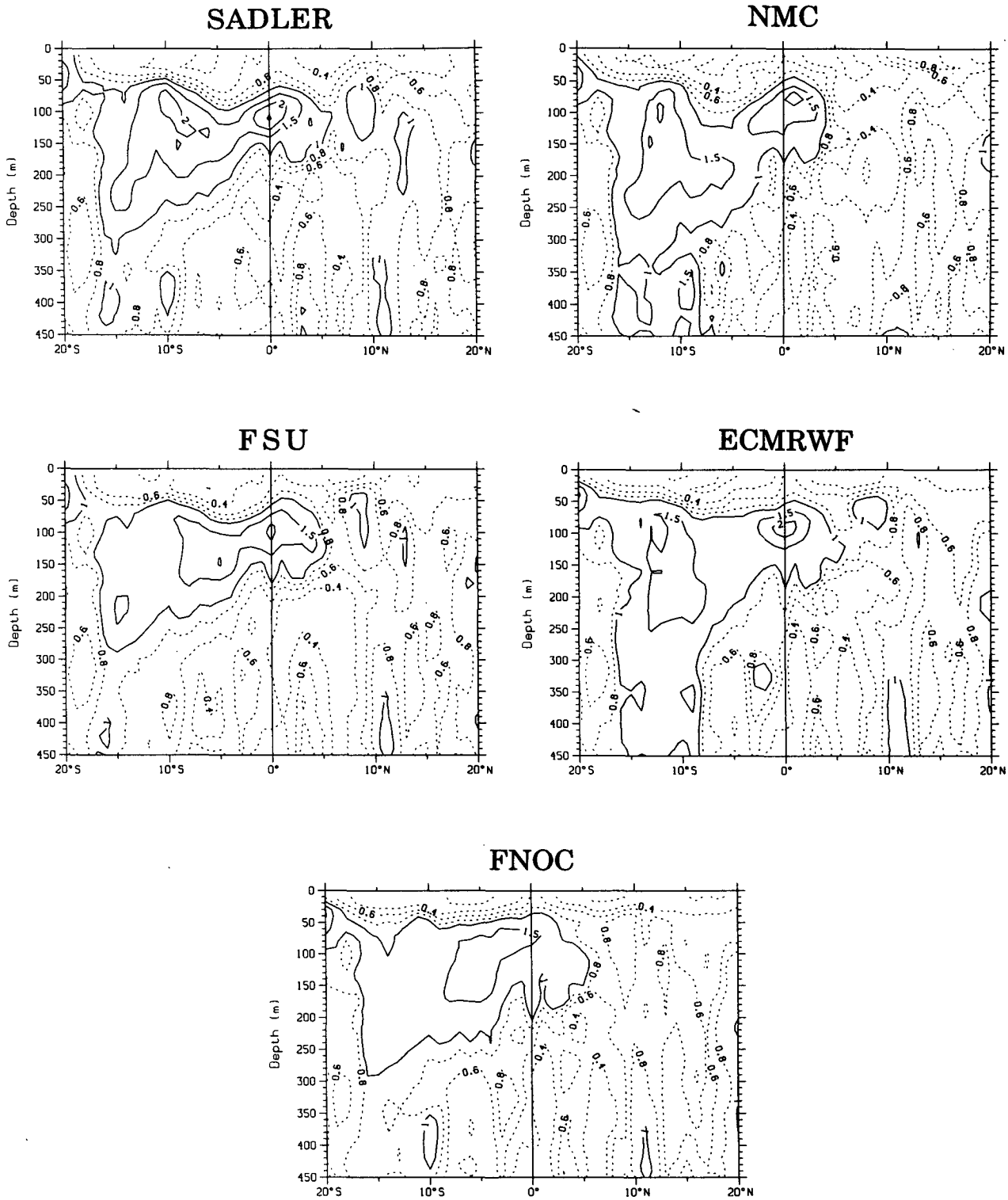

FIG. 13. As in Fig. 12 except for the central Pacific track.

SADLER and FSU have $S > 2$ over substantial distances. North of 3°N, skill decreases to at best marginal levels; NMC skill in the NECC range is very low (0.3). In the WP, there is at least marginal skill between 10°S and 10°N for each hindcast except NMC. Maximum skill values exceed 2. NMC skill is marginal or better

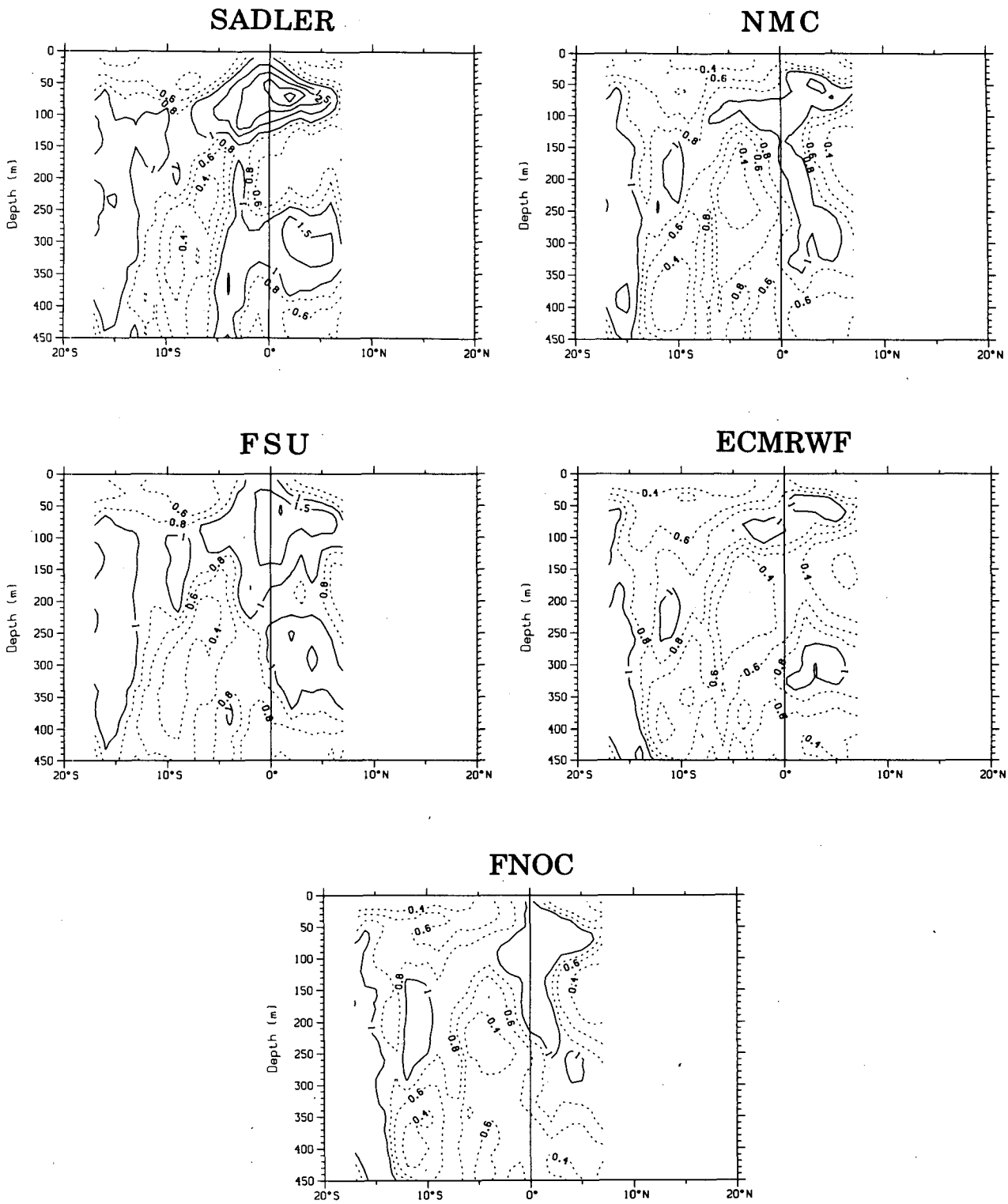

FIG. 14. As in Fig. 12 except for the eastern Pacific track.

only between 5° and 13°S and somewhat north of 10°N. There is a local minimum in skill in the southern part of the NECC region in every hindcast.

To somewhat oversimplify, the best temperature hindcast skill is found in the thermocline in every hindcast; except in the WP, skill is highest in the equa-

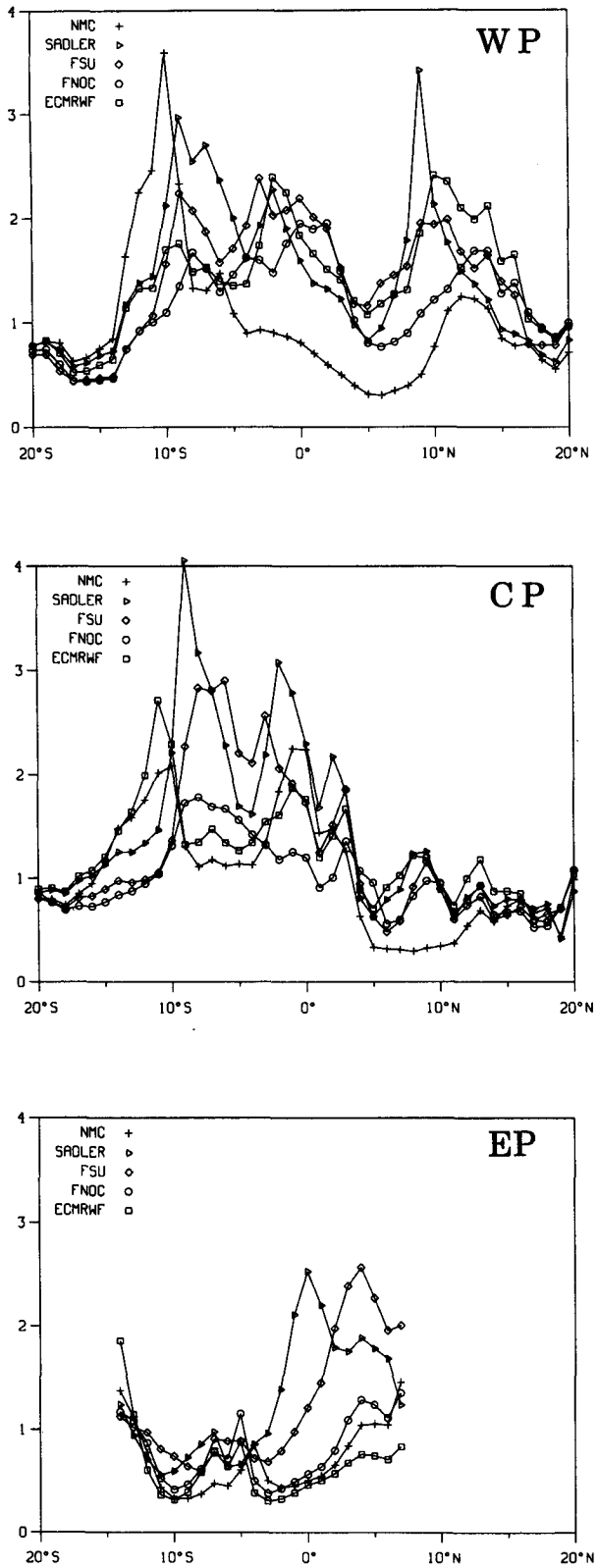

FIG. 15. Hindcast skill index for 0/450 m dynamic height. Top panel: western Pacific; middle panel: central Pacific; bottom panel: eastern Pacific. See text for discussion.

torial thermocline and next highest somewhere between 5° and 10°S. The highest skill values typically exceed 2.0, although ECMWF and FNOC do not attain this level anywhere in the EP or WP and NMC does not attain it in the EP. Dynamic height hindcast skill varies considerably between sections. Across the waveguide in the EP only SADLER has quantitative hindcast skill, in the CP SADLER and NMC sustain quantitative skill and the others are marginally skillful, while in the WP all but NMC are quantitatively skillful; as has been noted before, EP skill is the hardest to achieve. Comparison with the variance in the data indicates that waveguide dynamic height hindcast errors range between 3–5 dyn-cm (WP), 3–7 dyn-cm (CP) and 5–10 dyn-cm (EP); the estimated uncertainty in the XBT results is about 3 dyn-cm, so the best hindcasts produce differences only a little larger than the data uncertainty. Such performance in the waveguide is very good indeed.

6. Summary and discussion

Hindcast experiments with the primitive equation tropical Pacific ocean general circulation model used by Philander and Seigel (1985) have been performed using five different wind stress analyses for 1982–83, to investigate hindcast sensitivity to our uncertain knowledge of the wind stress over the tropical Pacific. We use the surface salinity, bucket SST, and XBT temperature data collected along three ship tracks, under the French–American ship-of-opportunity program, for comparison with model hindcast time series along these tracks. Although the monthly average wind stress fields have a number of qualitative similarities, the quantitative differences between analyses are considerable; the different hindcasts reflect these differences in a number of ways, and to differing degrees depending upon the hindcast variable of interest. Every hindcast reproduces the essential large scale ENSO behavior in the waveguide–surface warming in the second half of 1982, continuing warm into 1983 and cooling back in mid-1983.

The hindcasts of 0/450 m dynamic height variations within the equatorial waveguide were quite successful. Each wind stress analysis produced hindcasts with at least much qualitative similarity to the observations, and most had considerable quantitative skill along at least one of the ship tracks. In the WP and CP, the best hindcasts correlated with observations at about 0.9; in the EP they are above 0.8. In the WP and CP waveguide the smallest hindcast/data rms differences approach the estimated observational uncertainty of about 2–3 dyn-cm; in the EP the smallest differences rise to 4–5 dyn-cm. No hindcast always produced the smallest rms differences (see section 5), but the SADLER hindcast was consistently among the best and the FSU hindcast was only slightly less successful.

The distinctive EP equatorial dynamic height double peaks about five months apart (Fig. 2) have been in-

vestigated by several investigators, using linear, single-active-layer reduced gravity models. Tang and Weisberg (1984), using an idealized wind anomaly, showed that two peaks about 45 days apart at 100°W could be associated with the passage of a downwelling Kelvin wave and its (first meridional mode) Rossby reflection. However, such peaks are much too close together compared to the observations. They also noted that a time-varying wind anomaly provides a tunable way to produce two separate peaks. Inoue and O'Brien (1986), forced their reduced gravity model with the FSU wind analysis and found two peaks about 3 months apart, which they attribute to Kelvin waves excited by relatively small variations superimposed on the major westerly wind anomaly.

The XBT observations show that the second peak arose both from high upper layer temperature and also large changes in the vertical temperature structure in the lower thermocline and thermostad (Fig. 5). Thus a single baroclinic mode model could not reproduce important aspects of the observed variability, particularly during 1983 when highly baroclinic changes occurred, including those associated with the double peak. Although a multibaroclinic-mode model would be less inconsistent with the observed subsurface temperature variations, many modes would be needed to reproduce the complex thermal changes between 12° and 23°C in the thermocline. Further, a substantial amount of the dynamic height variability resulted from SST change; since SST changes do not bear any consistent relationship with thermocline depth changes, relatively complete thermodynamics must be a part of any model hoping to reproduce fully the observations.

Most of the model hindcasts (the exception being FNOC) did have large changes in vertical gradient structure during 1983. The double peak signal in the EP is reproduced to some degree in each hindcast, but the second peak is generally not produced for the correct reason; most of the hindcasts (especially NMC) produced it from excessively warm near-surface temperatures. The SADLER hindcast had vertical structure changes similar to those in the data during this late-1982 to early 1983 period, but differed considerably from the observations for much of 1982.

Dynamic height hindcast skill outside the equatorial waveguide is quite spatially variable (see sections 4 and 5). In the WP both north and south of the equator, the best hindcasts do as well as the best waveguide hindcasts: in the CP none of the hindcasts has skill in the southern part of the NECC region and even the best have only marginal skill near 10°N. But south of the equator, where very large changes occurred, there is generally good skill all the way to 15°S. The SADLER hindcast was best at reproducing the large southern hemisphere changes in both the CP and the WP. In the EP only FSU and SADLER have quantitative skill outside the waveguide, and there only north of the equator.

A very simple examination of the extent to which direct wind stress curl forcing of thermocline depth changes is taking place (via Ekman pumping) suggests that this can be a major factor in the dynamic height changes outside the waveguide; some of the changes in NECC transport and in SEC transport in the CP and WP appear to result from the large changes in wind stress curl which themselves arise substantially from the changes in the zonal stress within 10 degrees of the equator. Of course, adjustment outside the waveguide generally involves slower processes than within the waveguide, and adjustment from initial condition shock is still taking place at the end of these hindcasts, but we find that the strong stress analyses create sufficiently strong direct forcing to give clear Ekman pumping response. This indicates that the problems in hindcast skill in the NECC region are importantly affected by the deficiencies in the wind stress curl patterns implicit in the monthly mean stress analyses.

SST hindcast skill was more limited. The model ocean warmed and cooled roughly in phase with observations, particularly within the waveguide, and correlations with data are often above 0.5, but there is never quantitative hindcast skill, and even marginal skill is infrequent. The strong stress hindcasts (SADLER and FSU) tended to produce colder SST than was observed in the eastern and central equatorial Pacific when the SE trades were present, while the weaker stress analyses (NMC, FNOC and ECMWF) tended to have SST too high in the western and central Pacific. Thus unrealistic SST, and SST gradients, existed in all of the hindcasts much of the time.

Equatorial SST changes are determined by the competing interaction of many processes—horizontal and vertical advection, mixed layer depth changes, mixing and surface heat flux—so that it is a particularly difficult variable to hindcast. Both the vertical mixing and surface heat flux parameterizations require further investigation and improvement; under very light wind conditions the model SST values commonly approached 32°C; evidently the imposed minimum evaporative cooling (see Philander and Seigel 1985, section 3) is not always sufficient to produce realistic maximum SST values. We note that any parameterization of the surface heat flux in terms of bulk formulae (as opposed to a Haney (1974)-type empirical parameterization) will require surface wind speed information. As done by Philander and Seigel (1985), speed for heat flux calculations is taken to be the stress divided by (air density times drag coefficient times relevant wind component). Further, most quasibulk layer mixed-layer models require the kinetic energy input to the layer, which depends upon the magnitude of the wind stress. Clearly surface wind and wind stress uncertainty have a major influence on hindcast SST skill.

Subsurface temperature hindcast skill is good where temperature changes roughly are correlated with ther-

mocline depth changes. Where there are changes in the vertical thermal structure between the surface and the thermocline, hindcast skill is highly variable and often not high.

Sea surface salinity is very poorly hindcast. Both air–sea and zonal advective fluxes of salt and water contributed to large salinity changes observed in the ship-of-opportunity data. There is no parameterization of precipitation minus evaporation in the model physics, so any changes due to surface water flux are absent from the model. Further, the Philander and Seigel (1985) initial state (January 1982) of the model ocean does not have realistic surface salinity gradients, so the large observed advective changes could not be reproduced by the hindcasts. We can only speculate that the model mixing processes affecting salinity have eliminated most of the upper-ocean horizontal salinity gradients in the course of the Philander and Seigel (1985) spinup to the initial state used in these experiments. As salinity effects are not unimportant in the data, improvement of treatment of salinity in the model also deserves attention.

It is important to note that the different stress fields are not the direct output of any of the research or operational wind or pseudostress analyses; rather we, or others, have taken analysis products and converted them to wind stress fields. The choice of $C_d = 1.2 \times 10^{-3}$ for the SADLER and FSU conversions is not conventional, but is based on the fact that this value gave better hindcast results than did larger values, and is more consistent with the Large and Pond (1981) C_d estimates for tropical conditions. The choices made to convert FNOC winds to stress resulted in quite small stress values, despite the fact that the FNOC winds are not dramatically smaller than the other operational winds. These results indicate that hindcast SST is very sensitive to the magnitude of the zonal stress near the equator, and that off-equatorial variability is strongly affected by wind stress curl amplitude and pattern, so there are significant issues associated with how wind analyses ought to be converted to stress fields. At this time these issues are far from clear.

This study shows that major waveguide dynamic height changes like those that took place in 1982–83 can be acceptably hindcast with several of the available monthly mean surface stress analyses. The best hindcasts reproduced waveguide dynamic height nearly at the estimated uncertainty in the observations. The sea surface temperature and vertical temperature structure changes that occurred are large; considerable spatial resolution and inclusion of both hydrodynamic and thermodynamic physical processes in the upper ocean appears necessary to gain an understanding of these changes. Outside of the waveguide, wind stress curl has been found to play an important role in both observed and hindcast changes in dynamic height, so the rather poor hindcast skill in the NECC appears to be related to the very uncertain wind stress curl fields in this region. Generally the special research products (FSU and SADLER) have higher skill in this region, which presumably results from their better spatial resolution of the wind stress there. The FSU analysis hindcast generally has somewhat poorer correspondence with the data than the SADLER hindcast; we attribute this to the greater month-to-month and region-to-region changes in the FSU analysis, since the gross aspects of the two analyses are often similar.

It has been suggested that the genesis of the 1982–83 El Niño involved a westward propagating baroclinic disturbance that was seen well north of the equator in 1981 (White et al. 1985; Pazan et al. 1986; Inoue et al. 1987). We note that all of the hindcasts described here were initialized with simulated climatological January ocean conditions, which included no information from the Pacific in 1981. The fact that very good to excellent hindcasts of waveguide dynamic height were obtained here (sections 4 and 5) strongly suggests to us that the primary agent of the El Niño waveguide signal was the 1982–83 wind stress changes and that whatever variability was associated with the free evolution of 1981 subsurface conditions was at most of secondary importance. We note, however, that we cannot speak to any aspect of causation for the 1982–83 surface wind stresses; coupled models are required in order to address such issues.

Given the model sensitivity to surface forcing information which has been documented here, this cannot be regarded as a complete model validation exercise. However, although elements of the ocean circulation model physical parameterizations and the model initial conditions require improvement, the results reported here generally bracket the observations. Thus, this primitive equation model appears appropriate for several-year duration studies. No dramatic offsets exist to be corrected, and the "climate drift" problem, which affects atmospheric circulation model studies on this time scale, is not a major factor for ocean studies such as this. Instead we find a very clear need for (among other things) improved knowledge of the surface wind stress field over the tropical Pacific, if we are to achieve quantitative hindcast skill for the ocean thermal quantities of interest in the El Niño phenomenon.

Acknowledgments. The interest, support and assistance of S. G. H. Philander and R. Pacanowski, who made their model available and helped us set it up on the NBS/NOAA Cyber 205, saved us many months of effort and is gratefully acknowledged. The various wind fields were made available to us by J. O'Brien (FSU), N. Wells (ECMRWF), A. Seigel (NMC), J. Sadler (SADLER) and the Fleet Numerical Ocean Center of the US Navy (FNOC); thanks to all; it must be noted that all decisions concerning how to convert the FNOC, SADLER and FSU fields to stress were made by the authors. The ship-of-opportunity program was initiated by G. Meyers, W. White, J.-R. Donguy

and D. Cutchin and has been continued as a cooperative program by the Office de la Recherche Scientifique et Technique Outre-Mer and the Scripps Institution of Oceanography. Computer time to carry out the model experiments on the NBS/NOAA system was provided by V. Derr of NOAA/ERL; J. Coffee, J. Harper and the computer center staff and operators made many special efforts to assist our getting this accomplished in as timely a way as possible. The expert programming assistance of S. Hankin and M. Verschell at PMEL, and PMEL computing support were also essential. The U.S. TOGA Project Office provided partial start-up support, and subsequent partial support has been received from the NOAA EPOCS Program. The financial support and enthusiasm of E. Bernard, Director of PMEL, are very much appreciated.

REFERENCES

Barnett, T. P., and W. C. Patzert, 1980: Scales of thermal variability in the tropical Pacific. *J. Phys. Oceanogr.*, **10**, 529–539.

Bunker, A. F., 1976: Computations of surface energy flux and annual air–sea interaction cycles of the North Atlantic Ocean. *Mon. Wea. Rev.*, **101**, 1122–1140.

Busalacchi, A. J., and J. J. O'Brien, 1981: Interannual variability of the equatorial Pacific in the 1960's. *J. Geophys. Res.*, **86**, 10901–10907.

——, and M. Cane, 1985: Hindcasts of sea level variations during the 1982–83 El Niño. *J. Phys. Oceanogr.*, **15**, 213–221.

Firing, E., R. Lukas, J. Sadler and K. Wyrtki, 1983: Equatorial Undercurrent disappears during 1982–83 El Niño. *Science*, **222**, 1121–1123.

Goldenberg, S. B., and J. J. O'Brien, 1981: Time and space variability of tropical Pacific wind stress. *Mon. Wea. Rev.*, **109**, 1190–1207.

Halpern, D., D. E. Harrison, et al., 1982: Intercomparison of November 1979 Pacific tropical surface winds. Massachusetts Institute of Technology Dept. of Meteorology and Physical Oceanography, Tech. Rep. 82-1.

Haney, R., 1974: A numerical study of the response of an idealized ocean to large scale surface heat and momentum flux. *J. Phys. Oceanogr.*, **4**, 145–167.

Harrison, D. E., 1984: On the appearance of sustained equatorial westerlies during the 1982 Pacific warm event. *Science*, **224**, 1099–1102.

——, V. Cardone, J. J. O'Brien, D. Reynolds, J. Sadler and D. Wylie, 1984: Report of the ad hoc committee on surface wind and wind stress fields. Univ. Corp. for Atmos. Res., USTOGA 2, 49 pp.

Hellerman, S., and M. Rosenstein, 1983: Normal monthly wind stress over the world ocean with error estimates. *J. Phys. Oceanogr.*, **13**, 1093–1104.

Inoue, M., and J. J. O'Brien, 1986: Predictability of the decay of the 1982/83 El Niño. *Mon. Wea. Rev.*, **114**, 967–972.

——, W. B. White and S. E. Pazan, 1987: Interannual variability in the tropical Pacific prior to the onset of the 1982–83 El Niño. *J. Geophys. Res.*, (in press).

Kessler, W. S., and B. A. Taft, 1987: Dynamic heights and zonal geostrophic transports in the central tropical Pacific during 1979–84. *J. Phys. Oceanogr.*, **17**, 97–122.

——, —— and M. McPhaden, 1985: An assessment of the XBT sampling network in the central Pacific. Univ. Corp. for Atmos. Res., USTOGA 4, 62 pp.

Large, W. G., and S. Pond, 1981: Open ocean momentum flux measurements in moderate to strong winds. *J. Phys. Oceanogr.*, **11**, 324–336.

Levitus, S., 1982: *Climatological Atlas of the World Ocean.* NOAA Prof. Paper 13, 173 pp., 17 microfiche, U.S. Govt. Printing Office, Washington, DC.

Lukas, R., S. P. Hayes and K. Wyrtki, 1984: Equatorial sea level during the 1982–1983 El Niño. *J. Geophys. Res.*, **89**, 10425–10430.

Luther, D. S., and D. E. Harrison, 1983: Observing long-period fluctuations of surface winds in the tropical Pacific: initial results from island data. *Mon. Wea. Rev.*, **112**, 285–302.

McPhaden, M. J., A. J. Busalacchi, J. Picaut and G. Raymond, 1988: A model study of potential sampling errors due to data scatter around XBT transects. *J. Geophys. Res.*, **93**, 10 589–10 603.

Meyers, G., 1979: On the annual Rossby wave in the tropical North Pacific Ocean. *J. Phys. Oceanogr.*, **9**, 663–674.

Niiler, P. P., (Ed.), 1981: Tropical Pacific upper ocean heat and mass budgets. A research program outline. Hawaii Institute of Geophysics special publication, 56 pp.

Pacanowski, R. C., and S. G. H. Philander, 1981: Parameterization of vertical mixing in numerical models of tropical oceans. *J. Phys. Oceanogr.*, **11**, 1443–1451.

Pazan, S. E., W. B. White, M. Inoue and J. J. O'Brien, 1986: Off-equatorial influence upon Pacific equatorial dynamic height variability during the 1982–83 ENSO event. *J. Geophys. Res.*, **91**, 8437–8449.

Philander, S. G. H., and A. D. Siegel, 1985: Simulation of El Niño of 1982–1983. *Coupled Ocean-Atmosphere Models.* J. Nihoul, Ed., Elsevier, 517–541.

——, W. J. Hurlin and R. C. Pacanowski, 1987: Initial conditions for a general circulation model of tropical oceans. *J. Phys. Oceanogr.*, **17**, 147–157.

Rasmussen, E. M., and T. H. Carpenter, 1982: Variations in tropical sea surface temperature and surface wind fields associated with the Southern Oscillation—El Niño. *Mon. Wea. Rev.*, **110**, 354–384.

Rebert, J. P., J.-R. Donguy, G. Eldin and K. Wyrtki, 1985: Relations between sea level, thermocline depth, heat content and dynamic height in the tropical Pacific Ocean. *J. Geophys. Res.*, **90**, 11719–11725.

Sadler, J., and B. J. Kilonsky, 1983: Meteorological events in the central Pacific during 1983 associated with the 1982–83 El Niño. *Trop. Ocean-Atmos. Newslett.*, **21**, 3–5.

——, and ——, 1985: Deriving surface winds from satellite observations of low-level cloud motions. *J. Climate Appl. Meteor.*, **24**, 758–769.

Schopf, P. S., and M. A. Cane, 1983: On equatorial dynamics, mixed layer physics and sea surface temperature. *J. Phys. Oceanogr.*, **13**, 917–935.

——, and D. E. Harrison, 1983: On equatorial waves and El Niño. I: Influence of initial states on wave-induced currents and warming. *J. Phys. Oceanogr.*, **13**, 936–948.

Tang, T. Y., and R. H. Weisberg, 1984: On the equatorial Pacific response to the 1982/1983 El Niño-Southern Oscillation event. *J. Mar. Res.*, **42**, 809–829.

White, W. B., G. Meyers, J.-R. Donguy and S. Pazan, 1985: Short-term climatic variability in the thermal structure of the Pacific Ocean during 1979–82. *J. Phys. Oceanogr.*, **15**, 917–935.

Wyrtki, K., 1984a: The slope of sea level along the equator during the 1982/1983 El Niño. *J. Geophys. Res.*, **89**, 10419–10424.

——, 1984b: A southward displacement of the subtropical gyre in the South Pacific during the 1982–83 El Niño. *Trop. Ocean-Atmos. Newslett.*, **23**, 14–15.

——, and G. Meyers, 1975: The trade wind field over the Pacific. Part II: Bimonthly fields of wind stress, 1950–1972. University of Hawaii. Ref. HIG-75-2.

——, and B. J. Kilonsky, 1984: Mean water and current structure during the Hawaii-to-Tahiti shuttle experiment. *J. Phys. Oceanogr.*, **14**, 242–254.